N66 35940
(ACCESSION NUMBER) (THRU)
95 1
(PAGES) (CODE)
CR-54979 14
(NASA CR OR TMX OR AD NUMBER) (CATEGORY)
FACILITY FORM 602

NASA CR-54979

NASA

TECHNIQUES FOR MOUNTING AN ULTRASONIC TEMPERATURE D[illegible]CE

by

L. C. Lynnworth and E. H. C[illegible]nevale

prepared for

NATIONAL AERONAUTICS AND SPACE ADMINISTRATION

CONTRACT NAS3-6211

PARAMETRICS, INC.

GPO PRICE $ _____

CFSTI PRICE(S) $ _____

Hard copy (HC) 2.50

Microfiche (MF) .75

ff 653 July 65

NASA CR-54979

FINAL REPORT

TECHNIQUES FOR MOUNTING AN ULTRASONIC TEMPERATURE DEVICE

by

L. C. Lynnworth and E. H. Carnevale

prepared for

NATIONAL AERONAUTICS AND SPACE ADMINISTRATION

February, 1966

CONTRACT NAS3-6211

Technical Management
NASA Lewis Research Center
Cleveland, Ohio
Nuclear Systems Division
Miles O. Dustin

Parametrics, Inc.
221 Crescent St.
Waltham, Mass. 02154

ABSTRACT

In order to apply the ultrasonic method of temperature measurement to rocket thrust chambers, special mounting techniques had to be developed. It was necessary to mount the transducer in such a manner that any sound transmitted around the periphery of the chamber would not affect the gas temperature measurement.

A study of mounting methods applicable to Centaur and Nerva type combustion chambers showed that the acoustic short circuit problem can be overcome by using vane probes and a delay line mount. In certain cases, it may be possible to transmit across the exhaust gas, without separating the cooling tubes, as would be required for vane probes.

In addition to studying mounting methods, ultrasonic probes, including transducers and flanges, were designed, developed and installed on a small hydrogen/oxygen rocket engine at the NASA-Lewis Research Center.

Sound velocity was measured using an ultrasonic pulse technique up to ~6000°R. This measurement was accomplished in the small hydrogen/oxygen rocket engine, despite severe noise conditions, unmixed gases, and flow velocities nearly one-tenth the speed of sound. Measured sound velocities were in reasonable agreement with theoretical estimates for this rocket engine. Based on these experimental results, it was concluded that the ultrasonic pulse technique could be used to measure temperature in flowing hydrogen at high pressure, in the range required in the contract specifications, 1000 to 5000°R. Other related ultrasonic studies and experiments in high temperature gases and plasmas further support this conclusion.

TABLE OF CONTENTS

		Page
I.	SUMMARY	1
II.	INTRODUCTION	2
	A. Background	2
	B. Review of Sonic Thermometry	2
	1. Gases	2
	2. Liquids and Solids	3
	3. Exhaust Gas Temperature	3
III.	OBJECTIVES OF PRESENT WORK	4
IV.	GENERAL DISCUSSION OF MOUNTING METHODS	5
	A. Unmodified Thrust Chamber	5
	B. Propagation Through Cooling Tubes	5
	C. Propagation Through Gas Only	6
	D. Phased Arrays: Beam Pattern, Temperature Distribution	6
V.	MOUNTING METHOD A	7
	A. Probe and Mount Designs	7
	1. Vanes	7
	2. Delay Line Mounts	8
	3. Reinforced Cantilever Mounts	9
	4. Coiled Tube Mounts	9
	5. Bellows Mounts	9
	6. Metal "O" Ring Mounts	9
	7. Mounts Using Methods A Plus B	10
	8. Exhaust Gas Diagnostics Using Momentary Contact	10
	B. Test Results and Analysis	10
VI.	MOUNTING METHOD B	12
	A. Probe and Mount Designs	12
	B. Test Results and Analysis	13

TABLE OF CONTENTS (cont' d)

		Page
VII.	HYDROGEN/OXYGEN ROCKET ENGINE	15
	A. General Remarks	15
	B. Static Tests	15
	C. Dynamic Tests at NASA-Lewis	16
	1. First Series	16
	2. Second Series	17
VIII.	RELATED ULTRASONIC TEST RESULTS IN GASES	20
	A. Ultrasonic Propagation in Hydrogen	20
	B. Ultrasonic Temperature and Transport Property Determinations in Heated Gases and Plasmas	20
IX.	CONCLUSIONS	21
X.	RECOMMENDATIONS	22
XI.	APPENDICES	
	APPENDIX I	23
	A. Probe Design and Beam Pattern Evaluation	23
	1. Hydrogen	23
	2. Gases Other Than Hydrogen	27
	APPENDIX II	28
	B. Refraction Effects	28
	APPENDIX III	30
	C. Ultrasonic Measurement of Temperature Distribution By Means of Beam Steering	30
	1. Introduction	30
	2. Ultrasonic Measurements	30
	3. Differential Path Obtained With Movable Probes	31
	4. Local Temperature Near Wall	31
	5. Radial Temperature Distribution	31
	6. Axial Temperature Distribution	32
	7. Analysis of Data from Beam Steering Experiments-Shape Factor	32

TABLE OF CONTENTS (cont' d)

		Page
	APPENDIX IV	33
	D. Instrumentation for Analog and Digital Readouts as Functions of Gas Temperature	33
	1. Introduction	33
	2. Equipment	33
	3. System Characteristics	33
	4. Preliminary Calibration	35
	5. System Advantages	35
	6. Compensation for Probe Delays	36
	7. Transmitter Circuitry	36
XII.	REFERENCES	37
XIII.	ACKNOWLEDGMENTS	41

TABLE OF FIGURES

1a. Schematic diagram of fission reactor for nuclear rocket shows measurement location of ultrasonic temperature sensor.

1b. Mounting Methods A and B.

2. Velocity squared vs temperature in hydrogen.

3a. Extended array of phased transducers.

3b. Schematic of room temperature tests through air, using split thrust chamber to avoid acoustic short circuit.

3c. Schematic of focussed transducers mounted on hydrogen/oxygen rocket engine.

4. Variable air path, and assembly and exploded views of a prototype vane probe.

5. Schematic of ultrasonic sensor mount, using delay line between transducer and hydrogen/oxygen rocket engine test chamber.

6a, 6b. Assembly and exploded views of standard tubing and fittings, connected together in early model to demonstrate tubular delay line mounting concept.

6c, 6d. Assembly and exploded views of first water cooled tubular delay line mounts used in hydrogen/oxygen rocket engine tests, August 1965.

7. Reinforced cantilever delay line mount.

8a. Delay line mount utilizing standard high pressure fittings.

8b. Delay line mount utilizing standard thermowell.

9. Coiled tube gives ~1 ms delay.

10. Bellows mount.

11. Metal "O"-ring mount.

TABLE OF FIGURES (cont'd)

12. Pneumatically actuated probes for momentary contact gas diagnostics.

13. Centaur thrust chamber for studying acoustic short circuit.

14. Instrumentation for ultrasonic gas temperature measurement.

15. Muffle tube oven.

16. Oscillograms demonstrate electrical performance of analog output circuitry. Waveform sequence shows no degrading effects due to acoustic short circuit, for simulated temperatures of 1000 to 5000°R.

17. Brazed test panels.

18. Crystals inside cooling tubes yield increased ultrasonic transmission into test gas.

19a. Assembly view of second pair of water cooled tubular delay mounts used in hydrogen/oxygen rocket engine tests, August 1965.

19b. Exploded view, showing adjustable probe mounts for hydrogen/oxygen rocket engine studies.

20. Thick walled copper test section.

21. Typical waveforms observed during ignition and combustion tests at NASA-Lewis in August 1965.

22. Hydrogen/oxygen rocket engine combustion chamber with ports for ultrasonic sensors.

23. Teflon isolation mount.

24. Hydrogen/oxygen combustion chamber mounted on test stand.

25. Measurement of ultrasonic pulses despite severe noise in hydrogen/oxygen rocket engine tests at NASA-Lewis in January 1966.

TABLE OF FIGURES (cont'd)

26. Beam characteristics of circular piston. Dimensions shown are approximations suitable for estimating purposes.

27. Frequency-diameter nomogram.

28. Temperature vs d^2/λ, with d^2f as parameter.

29. Temperature vs d/λ, with df as parameter.

30. Increase in sound-pressure level along the normal axis of a piston generating constant acoustic power as a function of the ratio of piston diameter to wavelength of sound.

31. Directional radiation pattern from a vibrating circular piston showing the degrees off the normal axis at which the attenuation is 3, 6, 10, and 20 dB as a function of piston diameter over wavelength.

32. Sound velocity vs temperature in various gases.

33. Geometry and notation for analysis of refraction effects in exhaust gas.

34. Refracted angle as a function of gas temperature, nozzle angle θ_n and probe design temperature.

35. Beam steering using refraction effects to compensate for gas flow.

36. Ultrasonic measurement of local gas temperature near wall.

37. Ultrasonic measurement of radial temperature distribution.

38. Ultrasonic beam steered to different receivers.

39. Ultrasonic measurement of axial temperature distribution.

40. Analog output generator.

41. Ultrasonic thermometer calibration.

I. SUMMARY

In our previous studies, it was concluded that temperature measurement by the ultrasonic pulse technique appears applicable to the nuclear rocket engine exhaust gas.

In order to apply the ultrasonic method of temperature measurement to rocket thrust chambers, special mounting techniques had to be developed. It was necessary to mount the transducer in such a manner that any sound transmitted around the periphery of the chamber would not affect the gas temperature measurement.

There were two mounting methods appropriate to readily available nuclear rocket engine thrust chambers or similar structures, namely: (1) Method A in which the transducer elements protrude between the cooling tubes into the interior of the thrust chamber, and (2) Method B in which the transducers are located outside of the thrust chamber and in intimate contact with the cooling tubes.

A study of mounting methods applicable to Centaur and Nerva type combustion chambers showed that the acoustic short circuit problem can be overcome by using vane probes and a delay line mount. In cases where the reinforcement band thickness is comparable to the ultrasonic wavelength, the short circuit pulse propagates in a zig-zag or quasi-Lamb wave mode at a reduced velocity. When this reduced velocity is ~0.1 in./μsec, there is no short circuit problem above 800°R, since the gas borne signal arrives at the receiver first, before the short circuit pulse. In such cases, if a crystal array can be mounted directly against the cooling tubes, it may be possible to transmit across the exhaust gas, without separating the cooling tubes, as would be required for vane probes.

In addition to studying Methods A and B, it was also necessary to design, develop and install ultrasonic probes, including transducers and flanges, for a small Government furnished hydrogen/oxygen rocket engine. Dynamic tests were performed at NASA-Lewis Research Center.

In these tests, sound velocity was measured using an ultrasonic pulse technique up to ~6000°R. This measurement was accomplished, despite severe noise conditions, unmixed gases, and flow velocities nearly one-tenth the speed of sound. The ultrasonic determinations of sound velocity were in reasonable agreement with theoretical estimates for this small rocket engine. Based on these experimental results, it was concluded that the ultrasonic pulse technique could be used to measure temperature in flowing hydrogen at high pressure, in the range required in the contract specifications, 1000 to 5000°R. Other related ultrasonic studies and experiments in high temperature gases and plasmas further support this conclusion.

II. INTRODUCTION

A. Background

Satisfactory measurement of temperatures in rocket engines generally remains one of the most desirable, and yet one of the most difficult aspects in this field. Practical operation of a nuclear rocket engine, in particular, requires measurement and control of core temperature. One approach to this problem is to measure the average temperature of the working gas after it has been heated by passage through the core, as indicated schematically in Figure 1.

Measurement of high temperature gases has not kept pace with recent advances in high temperature technology. Although many theoretically feasible techniques of measuring high temperature gases have been suggested by a number of investigators, most of these need to be perfected and demonstrated before they can be accepted as reliable and be used on a routine basis. Furthermore, a technique applicable for one system may not be applicable for a different system. Thus, the specific requirements of a given system must first be considered before applying one or more of the many temperature measuring techniques that have been proposed.

B. Review of Sonic Thermometry

Determination of temperature from sound velocity measurements was suggested nearly 100 years ago by Professor Mayer.[1] The temperature dependence of the sound velocity may be measured in a gas, liquid or solid. Although the method is quite simple in principle, it has not been applied to high temperatures except in a few instances.[2-15]

1. Gases. Sonic thermometry in gases is based on the principle that in an ideal gas, sound velocity is proportional to the square root of temperature. Early work on sonic thermometry in gases was carried out by Suits[13] at General Electric in determining arc temperatures. In recent times it has successfully been applied to the measurement of gas temperature in an internal combustion engine,[14] various gases, and high intensity dc and ac arc plasma jets.[2] The techniques developed for sonic thermometry are also applicable, with some modification, to temperature measurements in liquids and solids.

2. Liquids and Solids. As examples of high temperature measurement of sound velocity in liquids and molten materials, the data of McDade et al[8] for water up to 1000°R, Hill and Ruoff's[9] measurements in molten indium to 1100°R, and McSkimin's data in molten tin up to ~1400°R may be cited.[10] Lehtinen[11] has reported sound velocity measurements in solidifying steel, at temperatures near ~3200°R. Macedo and Litovitz[12] studied molten boron trioxide up to ~3100°R.

Earlier ultrasonic thermometry work in solids was done in England in connection with reactor core temperature determination to 3200°R in the Dragon Project. Bell,[3] Thorne,[4] Hub,[5] Robins[6] et al have applied thin wire systems to the measurement of temperature. Parametrics, Inc. recently began a study of thin wire ultrasonic thermometry, to extend the useful range of this technique to 5000°R, including an experimental study of radiation effects in various wires irradiated at room temperature and annealed at elevated temperatures.[7]

3. Exhaust Gas Temperature. Parametrics, Inc. recently investigated an ultrasonic pulse technique for measuring the average gas temperature in a nuclear rocket engine.[15] This included a study of sound propagation in high temperature gases, particularly hydrogen, and the effects of the nuclear rocket engine environment on the ultrasonic sensors. A working model of a pulsed ultrasonic thermometer was also constructed.

Sound propagation studies included a theoretical analysis of the dependence of sound velocity on temperatures up to 5000°R, pressure, frequency, internal states, flow, boundary layers, and contaminants.

A major portion of the work concerned environmental studies. Here, sound propagation was evaluated while simulating various parameters of the nuclear rocket engine environment. The effects of high neutron and gamma radiation on piezoelectric transducers were measured in the MIT nuclear reactor. During a 15 hour ($> 5 \times 10^4$ sec) acoustically monitored test, the flux levels were: thermal neutron flux, $\sim 2 \times 10^{13}$ n/cm^2-sec; flux of 1 Mev or greater energy neutrons, $\sim 2 \times 10^{12}$ n/cm^2-sec; gammas, 0.7 Mev average, 1.5×10^8 R/hr $\approx 10^{14}$ Mev/cm^2-sec. Degradation of PZT-5 transducers was observed to be negligible under this flux. Geometrical and mechanical problems of conveying ultrasound to and propagating diametrically across a 1 to 2 foot hydrogen gas path were also considered. To determine the effects of vibration on the signal to noise ratio, an ultrasonic receiver and

test unit were subjected to audio frequency accelerations ranging up to $\pm$ 10g. From these various environmental studies, it was concluded that temperature measurement by the ultrasonic pulse technique appears applicable to the nuclear rocket engine exhaust gas.

III. OBJECTIVES OF PRESENT WORK

In order to apply the ultrasonic method of temperature measurement to rocket thrust chambers, special mounting techniques had to be developed. It was necessary to mount the transducer in such a manner that any sound transmitted around the periphery of the chamber would not affect the gas temperature measurement.

There were two mounting methods appropriate to readily available nuclear rocket engine thrust chambers or similar structures, namely:

1. Method A in which the transducer elements protrude between the cooling tubes into the interior of the thrust chamber, and

2. Method B in which the transducers are located outside of the thrust chamber and in intimate contact with the cooling tubes.

In addition to studying Methods A and B, it was also necessary to design, develop and install ultrasonic probes, including transducers and flanges, for a small Government furnished hydrogen/oxygen rocket engine. Static tests on this 2 in. diameter rocket engine combustion chamber were to be performed at Parametrics, Inc. Dynamic tests were to be performed at NASA-Lewis Research Center. The purpose of these tests was to simulate in part the noisy high temperature, high pressure environment of the nuclear rocket engine. Thus, the tests would provide valuable data relative to noise effects under high temperature, high pressure dynamic conditions.

IV. GENERAL DISCUSSION OF MOUNTING METHODS

Before discussing mounting methods in detail, the following general remarks are presented.

A. Unmodified Thrust Chamber

There are several approaches to mounting the ultrasonic sensor on a rocket nozzle. The most attractive approach is that in which there is no major modification of the nozzle. In this method the sensors would be mounted on the outermost retainer surface or reinforcement band. If an ultrasonic pulse of sufficient amplitude can be made to travel through the retainer material, cooling tubes and the exhaust gas in less time than around the periphery, or acoustic short circuit path, this method can be acceptable. If, on the other hand, the sound travels faster around the periphery than through the gas, the system can still be made to work if there is sufficient attenuation in the peripheral mode.

The velocity and attenuation of the short circuit path is a complex function of the material and configuration of the nozzle, and can only be understood properly by experimentation with the actual nozzle.

B. Propagation Through Cooling Tubes

The next approach in order of desirability is that of mounting the ultrasonic probes in intimate contact with the cooling tubing. This is referred to as Method B. In this method the ultrasonic pulse is isolated from the retainer wall which presents the peripheral path of least attenuation. Success will be achieved in this method if the complex sound path through cooling tubes, brazing alloy and mounting joints is such that the sound propagation is sufficiently attenuated or slowed down.

Any method that breaks the outer retaining wall must incorporate a high pressure seal between the acoustic probes and the wall. This pressure seal must be so constructed that the necessary acoustic delay and isolation are achieved.

C. Propagation Through Gas Only

The approach which generally has the highest probability of success is that designated as Method A. In this method the ultrasonic probe elements are placed between the cooling tubes so that they protrude into the interior of the thrust chamber. It has been shown[15] that these probe elements can be as narrow as one-tenth inch.

This method offers much more flexibility than those described above, since it is much easier to obtain increased transmission through the gas and decreased transmission through the rocket nozzle periphery. Again, a proper pressure seal is required which at the same time provides adequate acoustic isolation.

Figure 1a shows a schematic of a fission reactor for a nuclear rocket engine, and the ultrasonic sensor positions. Figure 1b illustrates the general concepts of mounting Methods A and B. Figure 2 is a calculated plot of sound velocity in hydrogen up to 5000°R, at pressures of 1, 10 and 100 atm.[15]

Some of the environmental difficulties encountered when instrumenting a nuclear rocket engine are indicated by Sutton.[16] The environment was partly described in our earlier work,[15] and more recent estimates of the environmental conditions and their effects on instrumentation are available in the literature.[17]

D. Phased Arrays: Beam Pattern, Temperature Distribution

Focussing, beam intensity, beam direction and beam directivity can be controlled to some degree by using a mosaic or array of crystal elements suitably phased. Phasing principles apply equally well to mounting methods A or B. As explained in the Test Results section, the acoustic short circuit problem may be neglected at sufficiently elevated temperatures, for reasonable separation of transmitter and receiver.

The simplest phasing arrangement is to excite all transmitting elements in phase. For transducers mounted on a circular reinforcement band, this leads to cylindrical waves which propagate essentially across the local diameter. Assuming a peripheral mode short circuit velocity of 0.1 in./μ sec, the transmitter and receiver, if symmetrical as in Figure 3a, can be quite extended, intercepting an arc of ~110° when the test gas is 5000°R hydrogen. Room temperature tests of this

concept could be conducted in air using a split chamber (Figure 3b). A tubular reflector could be used for pulse echo tests.

Cylindrical waves can also be used in combustor studies (Figure 3c), to take advantage of higher intensity focussed pulses. The focus need not be on the axis; it can be at the receiver, permitting the use of a small receiver, to reduce noise pickup. This approach is being evaluated in ultrasonic shock tube studies.[18] Tarnoczy[19] has recently reviewed some of the problems associated with focussing ultrasonic waves.

Appendix I presents equations, nomograms and sample calculations relative to probe design and beam pattern evaluation. Appendix II considers refraction effects as a function of temperature and nozzle geometry. Appendix III briefly describes the concept of ultrasonically determining temperature profiles by means of electrical or mechanical beam steering along different chords across the thrust chamber. Instrumentation is described in Appendix IV.

V. MOUNTING METHOD A

A. Probe and Mount Designs

1. Vanes. Assembly and exploded views of a prototype vane probe are shown in Figure 4. The plastic foam is used to restrict radiation to the vanes only. Thus the foam blocks the sound that ordinarily would be blocked by the cooling tubes. The crystal is a 2.5 in. diameter, 0.5 MHz PZT-5 disc. The vanes could also be driven by individual crystal segments excited in phase relationships appropriate to the desired radiation pattern. The vanes shown measure 0.1 in. x 1 in. x 1 in. More generally, each vane should be narrow enough so that dimpling of cooling tubes will not restrict coolant flow.

Several vane cross sections have been considered. A comparison of rectangular, double wedge and symmetrical airfoil shapes is shown in Table 1.

From this table it appears that a symmetrical airfoil, at zero angle of attack, would be the optimum shape. According to Hunsaker and Rightmire,[20] an airfoil of this shape will have very little flow

separation and, therefore, will produce the minimum disturbance to the flow and also will induce the least acoustic noise near the receiving probe. This is an important consideration since this noise will have to be filtered out by the readout system. If the probe is to be flush mounted then the probe shape will be such as to minimize the disturbance to the coolant tubes in the chamber wall.

Table 1

Comparison of Vane Shapes

Shape	Ease of Fabrication	Acoustic Noise Generated At Probe	Flow Disturbance	Stagnation Point Heating	Cross Sectional Radiation Area
Rectangle	Simple	High	High	High	High
Double Wedge	Medium	High	Medium	Low	Low
Symmetrical Airfoil	Difficult	Low	Low	Medium	Medium

---

2. Delay Line Mounts. In nozzle or thrust chamber structures where the reinforcement member is so thick with respect to ultrasonic wavelength that longitudinal waves (as distinct from zig-zag or quasi-Lamb waves) propagate around the periphery with little attenuation, a delay line mount is required so that the gas borne acoustic pulse is received before the unwanted short circuit pulse. Vane probes consisting of one or more vanes may be isolated from the thrust chamber using various delay lines, in order to avoid the problem of the acoustic short circuit. Tubular or bellows types are of relatively straightforward construction, typical designs being represented in Figures 5 to 11. Figure 5 shows a schematic of the delay line concept, but not the details of cooling passages. Cooling must be adequate to remove heat conducted from the ~5000°R hydrogen exhaust

gas, as well as that generated by gamma heating (substantially more than one watt/gram in some cases).[17] Figures 6a to 6d show both an early model tubular delay line and also more complicated constructions with cooling passages. These test mounts were constructed of copper, but for an actual installation on a nuclear rocket engine thrust chamber, stainless steel would be preferred, particularly an alloy similar to that used for the thrust chamber cooling tubes.

3. Reinforced Cantilever Mounts. To avoid the vibrations and large displacements of a cantilever mount, three supports at 120°, as illustrated in Figure 7, may be introduced without sacrificing any delay. The tubing may be mounted with standard high pressure fittings such as Swagelock or Parker, for tubing diameters up to 1 or 2 in., respectively (Figure 8a), instead of with flanges. Standard thermowells, cooled internally, would also be applicable in some cases (Figure 8b).

4. Coiled Tube Mounts. Very long delays can be coiled to conserve space. Figure 9 is a photograph of a 5 ft long tube coiled to a 6 in. diameter helix. In copper, this mount provided a delay of ~1 ms due to the establishment of a low velocity zig-zag wave in the wall of the tubing. The purpose of constructing a delay line mount with this much delay was to facilitate tests in room temperature air over a 1 to 2 ft path across the diameter of a Government furnished Nerva type thrust chamber. Normally, delay mounts of this size would not be required.

5. Bellows Mounts. Figure 10 shows another cantilever design, but here the cantilever is very short, ~1 in. compared to Figures 5 and 9. The use of a pressure-tight enclosure around the outside of the bellows substantially reduces the pressure gradient across the bellows, by about an order of magnitude in the present case, since a hole allows pressure equalization on both sides of the bellows.

6. Metal "O" Ring Mounts. Figure 11 illustrates metal "O" ring alternatives to bellows. Again, a pressure-tight enclosure is recommended, to avoid stressing the joints between adjacent "O" rings.

The above mounts, Figures 5 to 11, can be constructed entirely of metal, which is desirable in view of the radiation levels, temperature extremes and mechanical loads to be experienced.

7. Mounts Using Methods A Plus B. The required delay can be divided into two equal delay line mounts, or it can all be built into one vane probe mount, the other probe being quite short. This latter choice, in effect, combines mounting methods A plus B.

8. Exhaust Gas Diagnostics Using Momentary Contact. A variation on the theme of A, of possible interest in temperature profiling and other gas diagnostic studies, would utilize the momentary contact probing technique which has been used by Parametrics, Inc. for several years in measuring temperatures and transport properties of plasmas up to ~30,000°R.[2] Automatically controlled, pneumatically actuated probes, similar to the type illustrated in Figure 12, could be used.

B. Test Results and Analysis

To demonstrate that ultrasonic sensors could measure temperature when mounted according to Method A, variable gas path tests were conducted at room and elevated temperatures. Room temperature tests used single element and multi-element vane probes, Figure 4, and an air path adjusted to give transit times from 350 to 135 μsec, simulating transit times in a 2 ft hydrogen path at 1000 to 5000°R, respectively. An acoustic short circuit signal was introduced by mounting two transducers 3.14 ft apart (measured circumferentially) on a Government furnished Centaur thrust chamber, Figure 13. The improved working model instrumentation, Figure 14, was not affected by the attenuated and delayed short circuit acoustic pulse. Appendix IV describes the improved working model instrumentation, with analog and digital readout capability, the output being proportional to transit time.

Elevated temperature tests were conducted in the muffle tube oven shown in Figure 15. Path length was varied for a gas temperature of about 1000°R, yielding accurately controlled transit times of 350 to 135 μsec, to simulate transmission across 2 ft of 1000 to 5000°R hydrogen. This test (Table 2) conveniently demonstrated in three ways that the acoustic short circuit signal did not influence the ultrasonic measurement of temperature.

With the short circuit injected at ~375 μsec, the path was varied to yield hot gas transit times less than and greater than 375 μsec. For gas transit times <375 μsec, the analog and digital outputs, and the visual display of start and stop pulses and meter current pulses on

an oscilloscope, all clearly showed that circuit response was not influenced by the short circuit pulse. This demonstrated mounting Method A, at conditions simulating a 2 ft hydrogen path from ~1000 to 5000°R. For gas transit times > 375 μsec, the readouts were constant, proportional to the short circuit transit time around the periphery of the Government furnished rocket engine. This demonstrated that for hydrogen temperatures much below 1000°R, the delay line mounts discussed earlier would be required.

Table 2

Comparison of Parameters in Nuclear Rocket Engine and Simulation Test

Parameter	Nuclear Rocket Engine	Simulation Test
Gas	Hydrogen	Nitrogen
Gas Pressure, psia	600	15
Gas temperature, °R	1000 to 5000	1000
Probe separation, in.	24	2.8 to 6.3
Maximum transit time, μsec	335	335
Minimum transit time, μsec	150	150
Probe material	Tungsten	Fused Silica
Probe shape	Vane	Cylinder
Probe diameter, in.	2.5	0.5
Probe area, in.^{2}	0.5	0.2
Transmitting Frequency, kHz	500	500
Readout	Analog	Analog and Digital

Figure 16 is a sequence of oscillograms showing that at simulated temperatures of 1000 to 5000°R, the start and stop pulses are separated proportional to gas transit time and meter current pulse width is proportional to gas transit time. These pulses are not affected or degraded by the subsequent acoustic short circuit pulse.

VI. MOUNTING METHOD E

A. Probe and Mount Designs

As mentioned earlier, Method B, in principle, is preferred over A because in B, the probe elements do not need to be inserted between adjacent tubes. In Method B, transmission through both reinforcement bands and the tubes was studied, as well as through the tubes or joints alone.

Referring to Figure 13 again, the Centaur thrust chamber is approximately 3 ft diameter at the exit, 0.5 ft diameter at the throat, and 5 ft long. Commercially available Branson Type ZR ultrasonic transducers are shown clamped to a reinforcement band. This particular arrangement was used to measure the acoustic short circuit signal, and its effect on the measurement of gas temperature.

With this thrust chamber, it was found that with one transducer coupled to the outside of the tubes or reinforcement band, a second transducer suspended inside the thrust chamber could detect a weak pulse. However, when the second transducer was coupled to the outside at a point diametrically opposite the first transducer, the received pulse was too weak to be detected. As discussed elsewhere, larger arrays could partly offset the attenuation through the chamber walls, and may be of interest in future studies.

To determine whether improved coupling could substantially increase the received signal level, the 3 in. x 3 in. test panels shown in Figure 17 were fabricated of brazed copper tubing. It was found that the panel with two flat faces transmitted about 1.6 to 3.6 db more signal than the panel with only one flat face, at frequencies of 1 and 0.5 MHz, respectively. However, transmission through these panels was quite poor, the insertion losses being ~26 db per panel at 0.5 MHz. Two smaller units developed in our earlier work[15] are shown for comparison purposes.

It is to be noted that the cooling tubes, Figure 13, typically taper such that their diameter is approximately proportional to the local thrust chamber diameter. Thus, for chamber diameter ~4 to 6 ft, larger tubing diameters may be expected in some cases. With larger tubing, it may be practical to extend concept B to include mounting the transducer against the inside wall of the tube, as shown in Figure 18.

B. Test Results and Analysis

In Method B, the probes directly touch the cooling tubes. Therefore, the short circuit transit time around the periphery is important. If the path is through a reinforcement band, the path length is $(\pi/2)$ times the local nozzle diameter. If the path is through adjacent tubes, assuming round tubes, the path length is increased to $(\pi/2)^2$ times the local nozzle diameter. The "effective" path can be even longer, depending on the particular quasi-Lamb wave mode or zig-zag wave which propagates around the structure. For both Government furnished Centaur and Nerva type thrust chambers, the short circu velocity was found to be ~0.1 in./μsec for frequencies between 0.5 and 3 MHz, or less than half the bulk wave longitudinal velocity. Based on this measurement, one can readily calculate the temperature above which the gas borne signal will arrive before the peripheral signal.

At $0^\circ C = 491^\circ R$, the sound velocity in hydrogen is 1284 m/sec = 0.05 in./μs. At some elevated temperature T, the gas transit time τ_g across nozzle diameter D (in.) is

$$\tau_g = \frac{D}{0.05\sqrt{T/491}} = 440\, D/\sqrt{T} \ \mu s.$$

For an effective short circuit sound velocity of 0.1 in./μs, the short circuit transit time τ_{sc} is

$$\tau_{sc} = \frac{\pi D/2}{0.1} = 15.9\, D \approx 16\, D \mu s.$$

Equating τ_g and τ_{sc} and solving for T,

$$T = 760 \approx 800^\circ R.$$

Thus, at temperatures above $800^\circ R$, there should be no short circuiting problem, for geometries similar to the present Government furnished thrust chambers. Moreover, as temperature increases

from 1000 to 5000°R, τ_g becomes shorter and shorter relative to τ_{sc}. This permits very large transducer arrays for possible use at the higher temperatures. Assuming a nozzle diameter of D = 24 in., allowable transducer dimensions, measured circumferentially, are as follows:

Table 3

Allowable Transducer Dimensions on 24 in. Diameter Nozzle*

Temp. °R	τ_{sc} μs	τ_g μs	$\tau_{sc} - \tau_g$ μs	Circumferential Extent per Transducer in.	Intercepted Angle degrees
1000	375	333	42	4.2	20
2000	"	236	139	13.9	67
3000	"	193	182	18.2	87
4000	"	167	208	20.8	100
5000	"	149	224	22.4	108

*Values calculated for short circuit sound velocity = 0.1 in./μsec around nozzle periphery.

In cases where these large transducers could be used, signals would be substantially greater (see Appendix I) than predicted by assuming transducer areas of ~1 in.^{2}

The amplitude of the short circuit signal can be substantially attenuated by sandblasting, knurling or otherwise roughening the surfaces from which the zig-zag wave reflects. In this way, Method B may be applied to lower temperatures.

Using the Government furnished thrust chambers, transmission was attempted through regions where the local cooling tube diameter was ~1/4 in. or less. Transmission through one wall and an air path was detectable but very weak. Transmission through two walls and an intermediate air path could not be detected. These tests used 1/2" diameter transmitter and receiver transducers. To increase signal strength to detectable levels, larger area arrays would be required (Figure 3), or else one might insert the crystals inside the cooling tubes to provide a better acoustic path leading into the gas (Figure 18).

VII. HYDROGEN/OXYGEN ROCKET ENGINE

A. General Remarks

Theoretical performance of liquid hydrogen with liquid oxygen as a rocket propellant has been calculated by Gordon and McBride.[21] Experimental performance has been reported by Hersch,[22] who used gaseous hydrogen as the fuel and liquid and gaseous oxygen as the oxidant. In 1962, Hersch reported ultrasonic velocity measurements across a 3/4 in. gas path, using a frequency of 150 to 170 kHz. In the present work, the gas path was increased to 2 in., and the frequency was increased to ~0.5 MHz or greater.

In the present program, the main reason for testing the probes on a small hydrogen/oxygen rocket engine was to determine experimentally whether the ultrasonic sensor and system developed earlier[15] could be mounted on a noisy high temperature source, and successfully measure sound velocity and temperature despite the acoustic noise in the combustion chamber. It is to be noted that, because of combustion, the hydrogen/oxygen combustion chamber is noisier than the nuclear rocket engine.

B. Static Tests

Prior to preliminary dynamic tests at NASA-Lewis, various static tests were conducted at Parametrics, Inc. Sound velocity was measured in copper bar and tubing, and sound attenuation was measured in copper and brass bar stock. For tubing wall thicknesses comparable to λ, zig-zag propagation was established with velocity <0.1 in./μsec. These measurements were used in the design of tubular delay line mounts. Attenuation measurements at room temperature and 3 MHz showed that longitudinal wave attenuation was $\approx$ 1 db/in. in copper and brass. At lower frequencies, attenuation is lower. It was therefore concluded that copper or brass probes up to about 1 in. long would not substantially attenuate the acoustic pulses in the anticipated rocket engine studies.

Test sections and probe mounts were pressure tested, and also tested to assure that acoustic short circuit problems had been avoided.

In related work, longitudinal velocity was measured at 1 MHz in a 1 in. length of OFHC copper, to ~2300°R. Results (Table 4) may be used to analytically estimate changes in probe transit time for particular temperature distributions. Use of pulse echo techniques

to experimentally compensate for probe delays is indicated in Appendix IV.

Table 4

Longitudinal Velocity as a Function of Temperature in Copper

Temperature °C	°R	Longitudinal Velocity cm/μ sec	in./μ sec
25	500	0.475	0.187
200	850	0.470	0.185
400	1210	0.457	0.180
600	1570	0.445	0.175
800	1930	0.429	0.169
1000	2290	0.396	0.156

Figures 6c and d show water cooled probes which can be bolted together across the test section. Figure 19 shows a later version of flanged probe mounts, each mount being individually bolted to the test section.

C. Dynamic Tests at NASA-Lewis

1. First Series. Initial dynamic tests of the combustor chamber and acoustic probes were conducted at NASA-Lewis from August 10 to August 13, 1965 (see Figures 6, 19 and 20). Ultrasonic pulses were transmitted through air, helium and oxygen during preliminary combustor check out. Also, loading effects of the electrically conductive tap water on the ultrasonic transmission system were determined. Internal water cooling of the probes was discontinued due to these loading effects. Figure 21 shows a series of oscillograms taken during ignition and combustion.

Initial tests with the ultrasonic probes a few inches downstream of the combustor inlet were not fruitful in that the noise levels produced were about ten times higher than the expected signal level. Therefore, with the available instrumentation, no transmitted ultrasonic signals

were observed (upstream noise, Figure 21). It was concluded that in these initial dynamic tests, the ultrasonic sensors were too close to the inlet, where combustion was not complete.

Subsequent tests were conducted with the ultrasonic probes approximately one foot downstream of the combustor inlet. The first firing yielded a signal that could possibly be interpreted as the received ultrasonic pulse (right bottom trace, Figure 21). The total transit time, across the 2 in. path was ~51 μsec, corresponding to a sound velocity of ~3280 ft/sec. This velocity was lower than the expected value of ~5000 ft/sec. In Hersch's earlier work,[22] experimental sound velocities ranged from about 3500 to 5000 ft/sec. Unfortunately the first firing was considered "hard" (i.e., a late combustion or explosive start occurred due to accumulated gases) and the ultrasonic transmitter/receiver system failed to operate after the test. (It was later determined that the transmit transducer bond heated up and the transducer slipped off its center position along the probe).

The combustor was then fired with each transducer used independently as a receiver, in order to check the noise levels. Results showed very little noise (right middle trace, Figure 21). Since only the original transmitter transducer was inoperative, the results with the receiver transducer were significant in that the noise level was found to be sufficiently low to enable transmitted signals to be readily received. It should be noted that the receiver transducer was found to be operating satisfactorily after it was removed from the combustor.

It was generally concluded that further tests should be conducted with externally cooled ultrasonic probes and a longer combustor section. The new design was intended to provide more complete combustion at the sensor location, improved acoustic and mechanical isolation of the probes, simpler probe mounting and easier assembly and alignment of the system.

2. Second Series. A second series of dynamic tests was conducted at NASA-Lewis from January 17 to 21, 1966. In these tests, a 4 in. diameter, 1 ft long combustion chamber was used, with ports for ultrasonic sensors near each end and the middle of the chamber. Figure 22 is a photograph showing exploded and assembly views of the combustor, ultrasonic sensors and dummy inserts. Details of the ultrasonic sensor are given in Figure 23. Sensors were hydrostatically tested to 600 psi before final assembly and dynamic testing. A seal between the 7/8-14

threaded brass sleeve and the teflon isolator was obtained by tightening the lock nut. Generally, however, a more conventional seal would be preferred.

The test stand mounting of the combustor, sensors, nozzle, water cooling lines for the nozzle, and the pressure tap is shown in Figure 24. During firings, four water jets are directed at the combustor in the vicinity of the ultrasonic sensors.

Run durations were from 0.3 to 3.3 sec. Chamber pressure generally ranged from 75 to 235 psia, with peak pressures being several times greater than these values, depending on the variability of the fluorine/hydrogen hypergolic ignition conditions. Metered oxidant/fuel (O/F) ratios were from 1.8 to 7.1. For these O/F ratios, theoretical sound velocities estimated by assuming 100% combustion, and neglecting heat losses due to conduction and radiation, and neglecting cold gas pockets, range from 4980 to 6180 ft/sec. Theoretical maximum equilibrium temperatures calculated by Gordon[21] for these O/F ratios range from 3400°R for O/F = 1.8 to 6200°R for O/F = 7.1. Theoretically, a maximum temperature of 6270°R can be achieved at an O/F = 8. Certain neglected factors, when taken into account, reduce the calculated average temperature across the combustor diameter. Since the flow velocity is less than one-tenth of Mach 1, a diametrically extended cold O_2 gas pocket, for example, less than ~0.2 in. long (axially) can lead to a relatively low sound velocity measurement. It has been estimated by Hersch that ultrasonically measured average temperatures as low as room temperature would not be unreasonable, in view of the liquid oxygen oxidant, and observed departures from 100% mixing and combustion.

Each oscillogram shown in Figure 25 records a number of received ultrasonic pulses, despite the presence of severe noise. Several traces are seen in each oscillogram, because the exposure time is 0.1 sec and the pulse repetition frequency is 60 pps. Thus, each oscillogram not only gives the sound velocity at which a given pulse propagates, but also gives the fluctuations over a given time interval, such as 0.1 sec in the present case. The carrier frequency is about 0.6 MHz, in the upper oscillogram, and about 0.8 MHz, in the lower one. These frequencies are about half the unclamped crystal frequency (~1.5 MHz). When piezoelectric crystals such as those used in these tests are tightly bonded to a buffer rod, the resultant resonant frequency is substantially reduced, in general, depending on the nature of the bond, crystal size and acoustic impedance, and buffer rod size and acoustic impedance. Depending on damping, isolation and impedance considerations, the frequency can also be pulled by tuning

the pulsed oscillator. It is sometimes advantageous, with respect to signal to noise ratio, to operate the transducers somewhat off their resonant frequencies. In this way, vibration-induced oscillations of the crystals can be filtered out, while the desired ultrasonic signal passes through to the receiver circuitry.

In each oscillogram, the leading edges of received pulses generally arrive about 60 μsec after the start of the electrical transmitted pulse. The gas transit time is therefore 60 μsec less the delay through two 2 - 3/8 in. long copper probes, or 60-25 = 35 μsec, using the room temperature sound velocity in copper listed in Table 4. The sound velocity in the test gas is therefore 2 in./35 μsec = 0.057 in./μsec = 4770 ft/sec. In the bottom trace in Figure 25, the earliest leading edge is detectable about 55 μsec after the start of the main bang, corresponding to a gas transit time of 30 μsec, and a sound velocity of 2/30 = 0.067 in./μsec = 5550 ft/sec.

The measured sound velocities are in good agreement with the earlier experimental results of Hersch.[22] We further note that in a given run of a few seconds durection, sound velocity varies by about ± 400 ft/sec or ± 7.5%. (Because the ultrasonic technique offers response time in the microsecond range, Hersch has suggested the possibility of using ultrasonic pulses at high pulse repetition frequencies to study oscillating combustion processes, where the combustion oscillation frequency is in the kilohertz range). Because the instantaneous O/F of the test gas at the point of measurement is unknown, temperature cannot be determined from the measured sound velocity in this situation.

The most significant conclusion to be drawn from this hydrogen/oxygen rocket engine study is that the ultrasonic pulse technique has been successfully demonstrated at frequencies of about 1 MHz over a path length of 2 in., despite the severe noise conditions, turbulence, refraction and scattering at the boundaries between unmixed gases, departures from equilibrium, and flow velocities nearly one-tenth the speed of sound. It is seen that with respect to acoustic noise, the conditions simulated in the hydrogen/oxygen engine were much more severe than those expected in the hydrogen exhaust gas of a nuclear rocket engine thrust chamber. Nevertheless, the ultrasonic pulse technique provided reasonable measurements of sound velocity in the hydrogen/oxygen engine.

VIII. RELATED ULTRASONIC TEST RESULTS IN GASES

In related programs, Parametrics, Inc. has propagated ultrasonic pulses through many gases, at pressures from 0.1 atm to 10 atm, and from room temperature, ~500°R, to elevated temperatures, ~25,000°R. Some of these test results are relevant to the present work, and accordingly are summarized below. These applications also demonstrate the increasing scope of ultrasonic technology with respect to high temperature gas studies.

A. Ultrasonic Propagation in Hydrogen

Using a shock tube test section as the gas container, ultrasonic velocity, attenuation and beam spreading were determined at 0.5 and 1 MHz in hydrogen at room temperature, at pressures down to 0.1 atm.[23] Within the limits of these experiments the rotational relaxation times in room temperature hydrogen[24] were generally confirmed. There are also recent experimental and theoretical results[25] available for the vibrational relaxation times. On the basis of this recent theoretical and experimental work, it appears that in high pressure hydrogen, at 1000 to 5000°R, contributions to sound absorption will be due to the classical viscosity and thermal conductivity (Stokes-Kirchoff), plus molecular absorption due to vibration and rotation.

The classical contributions to sound absorption can be calculated with sufficient accuracy for the present purposes. Using this classical calculation, together with recent information and molecular relaxation times, the sound absorption in high pressure, high temperature hydrogen can be reasonably estimated. However, since the temperature dependence of the rotational relaxation time is as yet unknown, sound velocity and attenuation will have to be measured in high temperature, high pressure hydrogen as part of the final calibration of the ultrasonic thermometer.

B. Ultrasonic Temperature and Transport Property Determinations in Heated Gases and Plasmas

An ultrasonic (~1 to 3 MHz) pulse method, similar to that applied in the present work (except for differential path techniques[2]) has been used to measure both velocity and sound absorption in argon, helium, nitrogen and oxygen in the temperature range 500-2500°K. Muffle tube ovens such as that shown in Figure 15 have been used as the high temperature source. Preliminary measurements in the temperature range

12,500 to 25,000°R have been obtained only in argon and nitrogen. These gases were heated to the plasma state with dc and rf plasma generators.[26]

From the ultrasonic measurements, temperature and transport properties of argon and helium have been determined. Rotational collision numbers have been obtained as a function of temperature in oxygen and nitrogen, and are in reasonable agreement with the theoretical values given by Parker.[27]

In shock tube studies,[28] ultrasonically determined temperatures are in good agreement with temperatures calculated on the basis of measured shock speed, and are also in excellent agreement with temperatures determined spectroscopically. The temperature range has been 8,000 to 17,000°R. Recently, attenuation data has been obtained using both multiple echo and differential path techniques. From the attenuation data, transport properties have been calculated.

IX. CONCLUSIONS

In this program, gas temperature was measured using an ultrasonic pulse technique up to ~6000°R. This measurement was accomplished in a hydrogen/oxygen combustor, despite severe noise conditions, unmixed gases, and flow velocities nearly one-tenth the speed of sound. The ultrasonic determinations of temperature are in reasonable agreement with theoretical estimates for this combustor. Based on these experimental results, it is concluded that the ultrasonic pulse technique could be used to measure temperature in flowing hydrogen at high pressure, in the range 1000 to 5000°R. Other related ultrasonic studies and experiments in high temperature gases and plasmas further support this conclusion.

A study of mounting methods applicable to Centaur and Nerva type combustion chambers showed that the acoustic short circuit problem can be overcome by using vane probes and a delay line mount. In cases where the reinforcement band thickness is comparable to the ultrasonic wavelength, the short circuit pulse propagates in a zig-zag or quasi-Lamb wave mode at a reduced velocity. When this reduced velocity is ~0.1 in./μsec, there is no short circuit problem above 800°R, since the gas borne signal arrives at the receiver first, before the short circuit pulse. In such cases, if a crystal array can be mounted directly against the cooling tubes, it may be possible to transmit across the exhaust gas, without separating the cooling tubes, as would be required for vane probes.

X. RECOMMENDATIONS

It is recommended that the ultrasonic pulse technique be applied to temperature measurement under conditions more closely simulating those of a nuclear rocket engine. It appears that exhaust gas composition, temperature, pressure, flow velocity, test duration, noise and vibration can all be reasonably and simultaneously simulated in pebble bed heaters which are now available or under construction. Information on radiation effects can be obtained in separate experiments, if required.

APPENDIX I

A. Probe Design and Beam Pattern Evaluation

1. Hydrogen

Analysis of probes and beam patterns of interest in this work is relatively straightforward. The relevant equations are the well known formulas describing the pressure radiated by a circular piston,* and the formula for the speed of sound as a function of temperature, $v = \sqrt{\gamma RT/M}$ (see Figure 2). The purpose of this appendix is to combine these formulas and thereby derive nomograms for probe design and beam pattern evaluation in terms of frequency f, transducer diameter d and temperature T. Results are obtained first for hydrogen, and then for other gases.

Analysis may begin by determining whether the receiver is in the near field, far field, or in the transition zone between. The terms near field and far field, analogous to the Fresnel and Fraunhofer regions of optics, respectively, are not uniquely defined. Rather, they are defined according to the particular problem at hand. Kinsler and Frey[29] define the far field as distances where the intensity follows a $1/r^2$ dependence. With this definition, the far field equations apply at distances from the piston exceeding $d^2/2\lambda$, where λ = wavelength $\approx$ const. x $\sqrt{T}$ for a given frequency.

Allen and Weiner[30] define the end of the near field as that distance where the far field equation gives an axial intensity equal to the average intensity over the face of the piston. This definition locates the end of the near field at $\pi d^2/4\lambda \approx d^2/\lambda$, which distance overlaps and in fact is twice as far from the piston as Kinsler and Frey's far field criterion, $d^2/2\lambda$.

Close to the piston, off the axis, the field is quite complicated. This region has been analyzed in some detail by Stenzel[31], and his results are available in graphical form in the English translation of Rschevkin's book.[32] The axial field is more amenable to analysis, and it is readily shown that along the axis, pressure goes through a series of maxima and minima (nulls). The last null is located $d^2/8\lambda$ from the piston, and the last maximum, at $d^2/4\lambda - \lambda/4 \approx d^2/4\lambda$. Beyond $d^2/4\lambda$ the axial pressure falls off smoothly, and beyond $d^2/2\lambda$, it falls as $1/r$, and the

*Square and rectangular pistons are concisely treated by G. W. Swenson, Jr., Principles of Modern Acoustics, pp. 110-114, Boston Tech. Pub., Cambridge, Mass. (1965).

intensity, as $1/r^2$ (Figure 26).

The major lobe exhibits essentially no spread within $d^2/4\lambda$ of the piston. Beam intensity falls to zero at the angles $\theta = \pm \sin^{-1} 1.22/(d/\lambda)$. Total beam width between half power points (-3db) is $70/(d/\lambda)$ degrees, or approximately λ/d radians. It can also be shown that at the end of the near field,[30] the beam diameter between half power points is approximately 2 d (Figure 26).

The directivity for a plane piston radiator is $(\pi d/\lambda)^2$, and is called antenna gain in radar applications.

It is obvious that the above relations all involve the ratio d/λ, which in our case is temperature dependent.

In order to quickly estimate beam patterns as a function of temperature, it is convenient to develop several nomograms. Figure 27 is a log log plot of frequency f vs diameter d, for various df and d^2f products. The slopes of these df and d^2f lines are -1 and -2, respectively, as is readily shown:

$$df = \text{const.} \qquad d^2f = \text{const.}$$
$$f = \text{const.}/d \qquad f = \text{const.}/d^2$$
$$\ln f = \ln \text{const.} - \ln d \qquad \ln f = \ln \text{const.} - 2 \ln d$$
$$\partial \ln f/\partial \ln d = -1 \text{ (solid line)} \qquad \partial \ln f/\partial \ln d = -2 \text{(dashed line)}$$

Figure 28 is a plot of T vs (d^2/λ), for lines of const. d^2f, of slopes = -2.

Figure 29 is a plot of temperature T vs (d/λ), with df = const. Here one calculates the slopes of the df = const. lines as follows:

$$v = f\lambda = df/(d/\lambda) = \text{const.} \times \sqrt{T} = A\sqrt{T}$$

$$\frac{1}{2} \ln T + \ln A = \ln \text{const.} - \ln (d/\lambda)$$

$$\partial \ln T/\partial \ln (d/\lambda) = -2.$$

The purpose of these nomograms is twofold: First, one determines if the receiver is in the near field or far field, for a given f, d and T. (If within $d^2/4\lambda$, neglect beam spread. If beyond $d^2/4\lambda$, continue to analyze spreading). Second, if in the far field, one determines d/λ. Then

one proceeds to Massa's[33] Figures 30 and 31 to estimate relative gain and beam spreading.

To illustrate the use of Figures 27 to 31, consider this example:

Nozzle diameter	=	D	=	24 in.
Transducer diameter	=	d	=	0.5 in.
Frequency	=	f	=	1 MHz
Minimum temperature	=	T_1	=	$1000^\circ R$
Maximum temperature	=	T_2	=	$5000^\circ R$

To estimate beam shape and relative intensity, proceed as follows:

1. Using Figure 27 (or by calculation), obtain the products $df = 0.5$ MHz - in. $= 0.5$ in./μsec, and $d^2f = 0.25$ in.^{2}/μsec.

2. Using Figure 28, for $d^2f = 0.25$ and $T_1 = 1000^\circ R$, read $d^2/\lambda \approx 3.7$ in. Since $D = 24$ in. $>> d^2/\lambda$, conclude that receiver is in far field.

3. Using Figure 29, for $df = 0.5$ and $T_1 = 1000^\circ R$, read $d/\lambda \approx 8$.

4. Using Figure 30, for $d/\lambda = 8$, read axial pressure increase (relative to omnidirectional source) $\approx$ 25 dB.

5. Using Figure 31, for $d/\lambda = 8$, read:

Intensity Relative To Axial Intensity, dB	Degrees Off Axis, θ	Beam Diameter Y At Receiver, in.
-3	3.5	3.3
-6	5	4.5
-10	6	5.3
-20	8	6.9

The values Y in the third column are calculated with the equation:

$$Y \approx d + 2\,(D - d^2/4\lambda)\,\theta/57.3$$

where θ = degrees off axis.

Repeating the above procedure for $T_2 = 5000^{\circ}R$, we have:

1. $df = 0.5$, $d^2f = 0.25$.

2. $d^2/\lambda \approx 1.4$ in. << D, so again receiver is in far field, and more spreading is to be expected at this higher temperature.

3. $d/\lambda \approx 3.2 \approx 3$.

4. Gain ≈ 17 dB, or about 8 dB less than previous case.

5. For $5000^{\circ}R$, obtain:

Intensity Relative To Axial Intensity, dB	Degrees Off Axis, θ	Beam Diameter Y At Receiver, in.
-3	10	8.5
-6	13	11.0
-10	15	12.5
-20	21	17.4

Although the above tabulated results are admittedly only approximate, they do provide a reasonable estimate of beam shape and relative intensity. With respect to propagation across a gas flowing at approximately 0.07 times the speed of sound, such that the beam is carried downstream 0.07 D ≈ 1.7 in., it is clear that more directivity is preferable. In principle, increasing either d or f would increase directivity. In practice, however, since effects of turbulence and attenuation are more severe at higher frequencies, it is preferable to increase d, rather than f. A lower limit on f is imposed by S/N and rise time considerations.

As a third illustration, let us increase d to 3 in., keeping f = 1 MHz, and evaluate the beam at $T = 5000^{\circ}R$.

1. $df = 3$, $d^2f = 9$.

2. $d^2/\lambda \approx 40$ in. > D (or $D \approx d^2/2\lambda$).

3. $d/\lambda = 19 \approx 20$.

4. Gain = 33 dB.

5. For T = 5000°R, obtain:

Intensity Relative To Axial Intensity, dB	Degrees Off Axis, θ	Beam Diameter Y At Receiver, in.
-3	1.3	4.4
-6	2	5.1
-10	2.3	5.4
-20	3	6.1

In this case, the receiver is located in the transition zone between near and far fields, where $1/r^2$ spherical divergence is being established (Figure 26). The directivity is quite reasonable. This is clear if we assume a 3 in. diameter receiver positioned to receive maximum intensity under no flow conditions. For flow velocity = 0.07 times the speed of sound, this receiver still intercepts about one-third of the major lobe. Clearly, a better position would be downstream about 1.7 in., in which case part of the beam is intercepted under no flow conditions, and essentially all the beam, at maximum flow. The technique of locating the receiver downstream was used in the combustor studies at NASA-Lewis.

2. Gases Other Than Hydrogen

To use the nomograms (Figures 28, 29) with gases other than hydrogen, we may make use of the approximation that the speed of sound in the test gas (e.g., N_2, A, etc.) at temperature T is the same as in hydrogen at temperature T', where

$$T' = \left(\frac{\gamma M'}{\gamma' M}\right) T .$$

The primes denote values in hydrogen, and the unprimed symbols denote values in the test gas.

T' can also be obtained from the equation

$$T' = \left(\frac{V}{V'}\right)^2 T$$

where the V and V' are sound velocities in the test gas and hydrogen, respectively, at the same temperature (e.g., $0^{\circ}C$).

The equations relating T and T' may be solved graphically, Figure 32. As an illustration, if $T = 4000^{\circ}R$ in helium, the temperature in hydrogen yielding the same sound velocity is $T' = 2260^{\circ}R$.

If $T' < 500^{\circ}R$, one can extend the nomograms (Figures 28, 29) or extrapolate from them, to obtain d/λ. For example, if $T = 4000^{\circ}R$ in nitrogen, $T' = 270^{\circ}R$, which falls below the range plotted in the nomograms. However, for initial estimating purposes, the nomograms generally suffice nevertheless, if reasonable care is exercised in extrapolating.

It may be of interest to note that the slopes of the lines in Figure 32 are $\partial \ln v/\partial \ln T = 1/2$.

APPENDIX II

B. Refraction Effects

To analyze refraction effects as functions of hydrogen gas temperature and thrust chamber geometry, we may begin by considering the situation depicted in Figure 33. Gas flow velocity is neglected for simplicity in this analysis.

Let the incident velocity in the ultrasonic probe be v_1, and the angle of incidence, θ_1. The refracted velocity in hydrogen is v_2, and the refracted angle, θ_2. It is clear that, for a given nozzle angle θ_n, and for a given v_1 and θ_1, θ_2 is a function of temperature. Three cases will be treated: $\theta_n = 5^{\circ}$, 25° and 45°.

According to Snell's Law,

$$\frac{v_1}{\sin \theta_1} = \frac{v_2}{\sin \theta_2} .$$

Suppose the transmitting probe is designed for a nozzle of $\theta_n = 45^{\circ}$, such

that, at 5000°R, $\theta_2 = \theta_n = 45°$. Then $v_1/\sin\theta_1 = (0.4\ cm/\mu sec)/0.707 =$ const. $\equiv$ A. At temperatures other than 5000°R, $\theta_2 = \sin^{-1}(v_2/A) = \sin^{-1} B\sqrt{T}$, where $B = \sqrt{\gamma R/MA^2}$ = const. Thus, the refracted angle θ_2 depends on nozzle geometry (θ_n) and the ' sign temperature for diametrical sound propagation. θ_2 is independent of the vibration mode in the probe, that is to say, v_1 may be a shear wave or longitudinal wave velocity.

Accordingly, probes may be characterized, for the present purposes, in terms of θ_n and a design temperature T.

In Figure 34, the refracted angle θ_2 is plotted as a function of gas temperature, for $\theta_n = 5°$, 25° and 45°, and for design temperatures of 1000, 3000 and 5000°R.

Several conclusions may be drawn from this graph. First, refraction effects are minimized for small θ_n. That is to say, θ_2 can be made quite insensitive to temperature, as $\theta_n \longrightarrow 0$.

The second conclusion, on the other hand, is that for large θ_n, e.g., $\theta_n = 45°$, θ_2 is relatively sensitive to temperature. (Means of exploiting this sensitivity are suggested in Appendix III).

The third conclusion is that, independent of θ_n, sensitivity of θ_2 to changes in temperature can be minimized by designing for the maximum temperature of interest.

To further illustrate the magnitude of refraction effects, consider the case $\theta_n = 45°$. Suppose the temperature range to be covered by a particular sensor is 4000 to 5000°R. Let the design temperature tentatively be chosen as 4500°R. From Snell's Law we have $v_1/\sin\theta_1 = v_2$ (at 4500°R)/sin 45° = (0.38 cm/μ sec)/0.707 = 0.54 cm/μ sec. At 4000°R, $\theta_2 = \sin^{-1} B\sqrt{T} = \sin^{-1}(0.358/0.54) = 41.5° \approx 42°$. At 5000°R, $\theta_2 = 47.9° \approx 48°$. Thus, at T = 4500°R ± 500°R, $\theta_2 = 45° \pm 3° \approx \pi/4 \pm 0.05$ radians. For a 24 in. diameter path, the refracted ray is displaced approximately (24 in.) (.05) = ± 1.2 in. at the receiver, for temperature fluctuations of ± 500°R. For receiver dimensions of ~1 in., and beam diameters of ~3 in., beam displacement of ± 1.2 in. generally would not seriously degrade the performance of the ultrasonic thermometer.

If desired, refraction effects sometimes may be used to advantage to accomplish beam steering. Beam steering may compensate for gas flow, for example, in cases where $\theta_n = 0$, and due to geometrical restrictions, transmitter and receiver sensor ports are diametrically opposite, with no allowance for downstream drift of the sound beam (Figure 35).

APPENDIX III

C. Ultrasonic Measurement of Temperature Distribution By Means of Beam Steering

1. Introduction

In cases where measurement of average gas temperature does not adequately describe the temperature within an engine, combustor, nozzle or other device through which hot, inhomogeneous gas is flowing, the measurement of temperature distribution becomes desirable.

Depending on the temperature and other test conditions, and particular test objectives, thermocouples are sometimes adequate for measuring temperature distribution.

In some instances, various optical techniques have been applied. For example, the relative intensity of a particular spectral line may be measured along a number of parallel chords. In a sense, an average temperature is measured along different paths. From these data, temperature distribution is calculated by integrating the inverted Abel integral equation. Details of the measurements and calculations are given by Hörmann,[34] who, over thirty years ago, studied temperature distribution and electron density in free burning arcs, and more recently, by Maecker,[35] who measured dc arcs, by Pearce,[36] who studied a dc plasma jet, by Reed,[37] in his work on the induction-coupled plasma torch, and by Simon,[38] in her work on the emission, absorption and temperature distribution in the H_2 - O_2 flame of a Beckman burner.

2. Ultrasonic Measurements

Analogous to the above optical determinations of temperature distribution obtained from integrated intensity measurements over different optical paths (generally parallel paths), an ultrasonic determination of temperature distribution may be obtained from measurements of integrated transit times over different acoustic paths (not necessarily parallel paths).[39] The detailed effects of gas flow are neglected in this analysis, for simplicity of presentation.

3. Differential Path Obtained With Movable Probes

Sound velocity has been ultrasonically measured in molten materials[12] and also in heated gases and plasmas,[2] using differential path techniques wherein either a reflector or a probe is displaced in small increments along its axis. In our plasma work, for example, ultrasonically determined temperature distributions were in reasonable agreement with Reed's [37] spectroscopic results for a similar rf plasma. The possibility of adapting momentary contact, differential path techniques (Figure 12) to ultrasonic temperature profiling was suggested earlier (p. 10). In this appendix we are concerned with differential path techniques where the ultrasonic probes are either stationary, or if they move (i.e., rotate), their displacement is small compared to the beam's motion.

4. Local Temperature Near Wall

As a simple example of beam steering, consider the probes shown in Figure 36. The forked transmitter T reflects or steers two pulses outward at 90° from its axis, to two receivers R_1 and R_2 at distances X_1 and X_2 from T. The purpose of the differential path is to minimize boundary layer corrections to the measured transit times, providing a more accurate temperature measurement in a local region $\Delta X = X_2 - X_1$.

5. Radial Temperature Distribution

Radial temperature distribution may be computed from ultrasonic transit time measurements over a number of parallel chords, Figure 37a, or over a number of nonparallel chords, Figure 37b.

In Figure 37b, the sound beam can be steered across the different receivers by mechanical or electrical means. Mechanical means may consist of a rotating transducer assembly, or so-called refraction analyzer[40] (Figure 38a). Sound velocity can be determined by measuring the transit time to each receiver. Alternatively, sound velocity can be calculated from a measurement of the angle at which the refraction analyzer must be set to obtain a maximum signal amplitude at a particular receiver. To illustrate the sensitivity of this approach to ultrasonic thermometry, consider again the last example in Appendix II. For $\theta_1 = 45^\circ$, and $T = 4500^\circ R \pm 500^\circ R$, $\theta_2 = 45^\circ \pm 3^\circ$. To measure T to $\pm 1\%$ in this range, or approximately $\pm 50^\circ R$, requires measuring θ_2 to $\pm 0.3^\circ$. From Snell's Law, this is readily shown to correspond to measuring θ_1 to $\pm 0.1^\circ$, for $v_1 = 0.2$ in./μsec, assuming gas flow velocity

is known.

Electrically, beam steering may be accomplished with standard techniques for controlling the time delay inserted between the pulser and the crystals (Figure 38b).

6. Axial Temperature Distribution

Axial temperature distribution may be computed, in principle, from measurements over different parallel or nonparallel acoustic paths, Figures 39a and b.

It may be noted that, in principle, measuring both θ_1 for maximum signal, and pulse transit time, permits both temperature and flow velocity to be calculated.

7. Analysis of Data from Beam Steering Experiments-Shape Factor

Pearce[36] has tabulated shape factors (S) relating the measured intensity distribution to the temperature distribution. Analogously, ultrasonic shape factors can be computed for various assumed temperature distributions. The ultrasonic transit time across a given path is*

$$t = \int_0^x \frac{dx}{v(x)} \approx \sqrt{\frac{M}{\gamma R}} \int_0^x \frac{dx}{\sqrt{T(x)}} .$$

The actual path will generally not be straight, but the effects of refraction can be accounted for to a good approximation by the methods of ray acoustics,[41] provided the radius of curvature of the refracted ray is much greater than the ultrasonic wavelength.

*Approximation shown is valid to the extent M and γ are not functions of x. See Figure 2.

APPENDIX IV

D. Instrumentation for Analog and Digital Readouts as Functions of Gas Temperature

1. Introduction

The analog output circuit described in Ref. 15 was redesigned and modified to operate with transit times associated with hydrogen temperatures in the range of 1000 to 5000°R over a 2 ft gas path. For demonstration purposes, the analog output was measured on a 0-5 volt dc meter. A digital output, consisting of an electronic timer which measured the acoustic pulse transit time, was also demonstrated.

2. Equipment

The working model instrumentation, Figure 14, consists of the following commercial equipment:

Arenberg Pulsed Oscillator	PG-650C
Arenberg Preamplifier	PA-620B
Lambda Power Supplies	Model 28

3. System Characteristics

a) General

The transit time is measured as the elapsed time between the acoustic pulse generation and reception, and is therefore the time required for the acoustic pulse to propagate through the gas plus probe and electrical delays. Transit time is measured as the interval during which the meter side of the flip-flop in the Analog Output Generator, Figure 40, is in a conducting state.

b) Detailed Operation of Output Circuitry

To demonstrate the model in air, 500 kHz was chosen as the ultrasonic frequency.

The pulsed oscillator drives the transmitter crystal at 500 kHz burst frequency, and at the same time switches the meter side of the

flip-flop to the conducting state. After the ultrasonic pulse travels through the gas, it generates a signal of at least 0.1 mv p-p in the receiver crystal. This signal is amplified by the tuned receiver preamplifier with ~50 db gain, giving a 500 kHz burst of received signal of 30 mv p-p or more at the output of the PA-620B.

This signal is fed into a transistorized pulse detector and amplifier circuit which yields a 22.5 volt positive trigger pulse when the leading edge of the receiver signal is detected. Adjustment of circuit parameters allows the pulse forming circuits to detect the optimum point on the received pulse for various signal-to-noise ratios. The third cycle of the received signal burst was detected during the demonstration of the working model. The pulse generated by the detecting circuitry is used to trigger the flip-flop after being fed through a variable gain pulse inverter stage. This trigger pulse restores the meter side of the flip-flop to its nonconducting state. Therefore, the flip-flop conducts current only during the transit time of the acoustic pulse. Assuming idealized circuit elements, the current through the flip-flop for one period, $i_{ff}(t)$, may be represented as:

$$i_{ff}(t) = \begin{cases} I_o & \text{when } \delta < t \leq \tau + \delta \\ 0 & \text{when } \tau + \delta < t \leq T + \delta \end{cases} \tag{1}$$

where τ = transit time of acoustic pulse through gas

T = period of acoustic pulse burst

δ = constant dependent on the arbitrary choice of a time origin

I_o = pulse current, fixed by circuit parameters.

This waveform repeats every period, so that the current through the flip-flop is a pulse train, where the constant amplitude current pulses have a width equal to the transit time of the acoustic pulse, and where the time interval between the successive pulse leading edges is fixed by the pulsed oscillator repetition rate. The meter time constant is such that it responds only to the dc component at the voltage across it. This voltage across the meter is obtained by allowing the flip-flop current to flow through a fixed resistor of value R ohms. Therefore, the meter indication $V_m(t)$ is obtained as the constant term in the Fourier expression of $i_{ff}(t)$ over successive pulses, where the change in transit time between successive

acoustic pulse bursts in a small fraction of the instantaneous transit time.

$$V_m(t) = \frac{R}{T} \int_{\delta}^{\tau + \delta} i_{ff}(t)\ dt\,. \qquad (2)$$

Substituting Eq. (1) into Eq. (2) we have

$$V_m(t) = \frac{R}{T} \int_{\delta}^{\tau + \delta} I_o\ dt + \frac{R}{T} \int_{\tau + \delta}^{T + \delta} (0)\ dt = \frac{I_o R}{T}\ \tau\,.$$

Therefore the meter deflection is directly proportional to transit time τ. By jointly adjusting the 20K meter sensitivity potentiometer and the pulse repetition frequency, the sensitivity of meter deflection may be controlled. The acoustic pulse transit time may also be measured on an electronic counter for greater accuracy. A Hewlett-Packard type 523-B Electronic Counter-Timer was used to measure transit time to $\pm$ 1 μsec in a demonstration of the working model, corresponding to transit time accuracies of better than 1% for τ = 150 to 335 μsec.

4. Preliminary Calibration

Figure 41 shows a plot of voltage read on the meter vs transit time of the ultrasonic pulse. Simulated hydrogen exhaust gas temperature is also indicated.

5. System Advantages

The primary advantage of this new system over that reported in Ref. 15 is that the present unit is more stable with respect to time. With the new system, the analog output voltage varied about 0.8% over the course of six hours for a fixed simulated temperature. An acoustic short circuiting signal injected into the receiver at a 375 μsec delay after the transmitted pulse did not degrade performance in the simulated 2000 to 5000°R range despite the short circuiting signal amplitude being 30 db above the amplitude of the acoustic pulse travelling through the gas. Below simulated temperatures of about 2000°R, operation of the readout circuitry is satisfactory provided the short circuiting

signal level is not unrealistically large. The short circuiting amplitude could be sufficiently reduced in the actual device by sandblasting the outside surface of the nozzle, creating a rougher, acoustically attenuating surface finish. This would prevent the acoustic short circuit from degrading the performance of the readout system.

Operation of this system is illustrated in Figure 16, which shows important waveforms in the circuit.

6. Compensation for Probe Delays

In order to compensate for the probe delays, a pulse-echo system could be used. For example, at the same time as the ultrasonic pulse is fired, a higher frequency (about 10 MHz) pulse is also transmitted. This second pulse will reflect off the probe-gas interface and travel back to the transmit crystal. When this pulse is detected, it is used to trigger the flip-flop and start the transit time count. This compensates for the delay in both probes (if identical) since double the transit time of one probe is utilized in this pulse-echo technique.

7. Transmitter Circuitry

It was found that the larger 2-1/2 inch diameter crystals used in conjunction with the vane probes are more effectively excited through use of a buffer amplifier,[18] which isolates their much higher capacitance from the Arenberg PG-650C Pulsed Oscillator. It has also been found that a thyratron pulser provides a relatively simple transmitter whose output circuit can be tuned to resonate with the crystal under pulse conditions.

XII. REFERENCES

1. A. M. Mayer, Phil. Mag. 45, 18 (1873).

2. E. H. Carnevale, H. L. Poss and J. M. Yos, "Ultrasonic Temperature Determination in a Plasma," in Temperature - Its Measurement and Control in Science and Industry (Reinhold Publishing Corp., New York, Vol. 3, Part 2, p. 959, 1962); E. H. Carnevale, G. S. Larson and L. C. Lynnworth, J. Acoust. Soc. Amer., 35 (11) 1883 (Nov. 1963); 36 (9) 1678-1684 (Sept. 1964); 36 (10) 1999 (Oct. 1964); G. S. Larson, R. N. Lawson and L. C. Lynnworth, ISA Trans. (1966); "Ultrasonic Measurements From 1000 to 10,000°K," L. C. Lynnworth and E. H. Carnevale, presented at 5th Congres Int'l D' Acoust., Liège, Belgium, Sept. 1965. Also see J. Apfel, Rev. Sci. Instr. 33 (4) 428-430 (Apr. 1962).

3. J. F. W. Bell, Phil. Mag. (8) 2, 1113-1120 (1957); Dragon Project Rpts. (Oct. 1960); Proc. 4th Int. Cong. Acoust., J52, Copenhagen, (1962).

4. E. A. Thorne, Proc. 4th Int. Cong. Acoust., P. 23, Copenhagen (1962); Temperature Measurement by Sonic Methods, presented at Inst. of Phys. and the Phys. Soc., and the Soc. Instr. Tech. Conf. on the Measurement of High Temperature, London (11-13 May 1964).

5. D. R. Hub, Proc. 4th Int. Cong. Acoust., J51, Copenhagen, (1962).

6. P. J. Robins, Industrial Electronics 3 (10) 482 (1965); Modern Refrig. 68 (803) 131 (1965).

7. See progress reports under NAS3-7981, Ultrasonic Temperature Measuring Device, NASA-CR-54780 (Oct. 1965) and CR-54896 (Jan. 1966), by E. H. Carnevale, L. C. Lynnworth and S. L. Klaidman.

8. J. C. McDade, D. R. Pardue, A. L. Gedrich and F. Vrataric, J. Acoust. Soc. Amer. 31 1380 (1959), in R. C. Weast (Ed.), Handbook of Chemistry & Physics, 45th ed., Chem. Rubber Co., Cleveland, pp. E28, E29 (1964).

9. J. E. Hill and A. L. Ruoff, Rev. Sci. Instr. 36 (10) 1465 (1965).

10. H. J. McSkimin, J. Acoust. Soc. Amer. 31 111(A), 287 (March 1959).

XII. REFERENCES (cont'd)

11. A. Lehtinen, Vortrag Nr. 7, 27 Intern. Gießereikongr., Zurich (1960).

12. P. Macedo and T. A. Litovitz, Phys. Chem. Glasses 6, (3), 69-80 (1965).

13. C. G. Suits, Physics 6, pp. 190-202 (June 1935).

14. J. C. Livengood, T. P. Rona and J. J. Baruch, J. Acoust. Soc. Am., 26, p. 824 (1954).

15. E. H. Carnevale, L. C. Lynnworth and G. S. Larson, NASA CR-54339 (Feb. 1, 1965).

16. G. P. Sutton, Rocket Propulsion Elements, 3rd ed., Wiley, New York, p. 464 (1963).

17. See, for example, IEEE Trans. on Nuclear Science, NS-13, (1) (Feb. 1966), especially J. A. Swartout, "Instrumentation and Nuclear Power," and F. S. Mallory, R. L. Ramp and G. A. Gilmour, "NERVA Nuclear Reactor Instrumentation."

18. E. H. Carnevale et al, "Shock Tube Research-Astrophysical Quantities," Quarterly Progress Rpts. under AF 19(628)-5053 (1966).

19. T. Tarnoczy, Ultrasonics 3, (3) 115-127 (July-Sept. 1965).

20. J. C. Hunsaker and B. G. Rightmire, Engineering Applications of Fluid Mechanics, pp. 196-197, McGraw-Hill, New York (1947).

21. S. Gordon and B. J. McBride, NASA Memo 5-21-59 E (June 1959).

22. M. Hersch, NASA TN D-1192 (March 1962); TN D-2169 (Feb. 1964).

23. Parametrics, Inc., "Ultrasonic Study Program and Transducer Assembly" (April 1966).

24. H. O. Kneser, "Relaxation Thermique dans les Gaz," pp. 40-61, especially Fig. 7, p. 62, in D. Sette, (Ed.), Dispersion and Absorption of Sound by Molecular Processes, Academic Press, New York (1963).

25. J. H. Kiefer and R. W. Lutz, J. Chem. Phys. 44 (2) pp. 658-672, especially Fig. 5, p. 671 (15 Jan. 1966); J. B. Moreno, Phys. of Fluids 9 (3) pp. 431-435 (March 1966).

26. E. H. Carnevale, G. S. Larson, L. C. Lynnworth, C. A. Carey, M. D. Panaro and T. Marshall, "Experimental Determination of Transport Properties of High Temperature Gases," prepared for NASA, Office of Advanced Research and Technology (1966).

27. J. G. Parker, Phys. of Fluids 2, p. 449 (1959).

28. E. H. Carnevale, C. A. Carey and G. S. Larson, "Experimental Determination of the Transport Properties of Gases," Tech. Rpt. AFML-TR-65-141 (Aug. 1965).

29. L. E. Kinsler and A. R. Frey, Fundamentals of Acoustics, 2nd Ed., pp. 169-177, Wiley, New York (1962).

30. C. H. Allen and S. D. Weiner, "Study Directed Toward Optimization of Operating Parameters of the EMAC Probe for the Remote Measurement of Atmospheric Parameters," AFCRL-63-596, pp. 52, 53, 54 (Sept. 1963).

31. H. Stenzel, Leitfaden zur Berechnung der Schallvorgänge (Guide to Calculating Sound Phenomena) Berlin (1958). See also Ref. 40, Sect. 44, pp. 12-19.

32. S. N. Rschevkin, A Course of Lectures on the Theory of Sound (1960), translated by O. M. Blunn, MacMillan Co., New York, Chap. XI, (1963).

33. F. Massa, Proc. IEEE 53 (10) pp. 1363-1371 (Oct. 1965).

34. H. Hörmann, Z. Phys. 97 pp. 539-560 (1935).

XII. REFERENCES (cont'd)

35. H. Maecker, Z. Phys. 136 119-136 (1953).

36. W. J. Pearce, Plasma Jet Temperature Study, WADC Tech. Rpt. 59-346 (Feb. 1960); "Plasma-Jet Temperature Measurement," in P. J. Dickerman (Ed.), Symp. on Optical Spectrometric Measurements of High Temperatures, Univ. of Chicago, 1960, 125-169, Univ. of Chicago Press (1961).

37. T. B. Reed, J. Appl. Phys. 32 (5), 821-824 (May 1961).

38. L. Simon, Optik 19 (12), 621-639 (1962).

39. L. C. Lynnworth, Mater. Eval. 24 (1) p. 55 (Jan. 1966); L. C. Lynnworth and E. H. Carnevale, "Ultrasonic Testing of Solids at Elevated Temperatures," to be presented at the Fifth International Conference on Nondestructive Testing, Montreal, Canada (May 21-26, 1967); T. Malim, Iron Age 195 (17) 75-77 (April 29, 1965).

40. R. C. McMaster, Nondestructive Testing Handbook, Vol. 2, Section 43, p. 22, Ronald Press, New York (1959).

41. See, for example, Physics of Sound in the Sea, Part I, Chap. 3, National Research Council, PB 111202.

XIII. ACKNOWLEDGMENTS

The authors gratefully acknowledge the technical guidance of M. O. Dustin, and the cooperation of M. Hersch and other NASA-Lewis personnel without whose assistance the successful conduct of the hydrogen/oxygen rocket engine tests would not have been possible. Thanks are also due to NASA personnel who made available Centaur and Nerva type thrust chambers, facilitating the studies of various mounting methods.

With appreciation, the authors also acknowledge the efforts of personnel at Parametrics, Inc., including R. N. Lawson's contributions to the analog output circuitry and Appendix IV, and the contributions of S. L. Klaidman, L. J. Remington, Jr., and B. J. Spencer to preliminary static testing of the hydrogen/oxygen rocket engine, and testing and demonstrating of mounting methods and the working model.

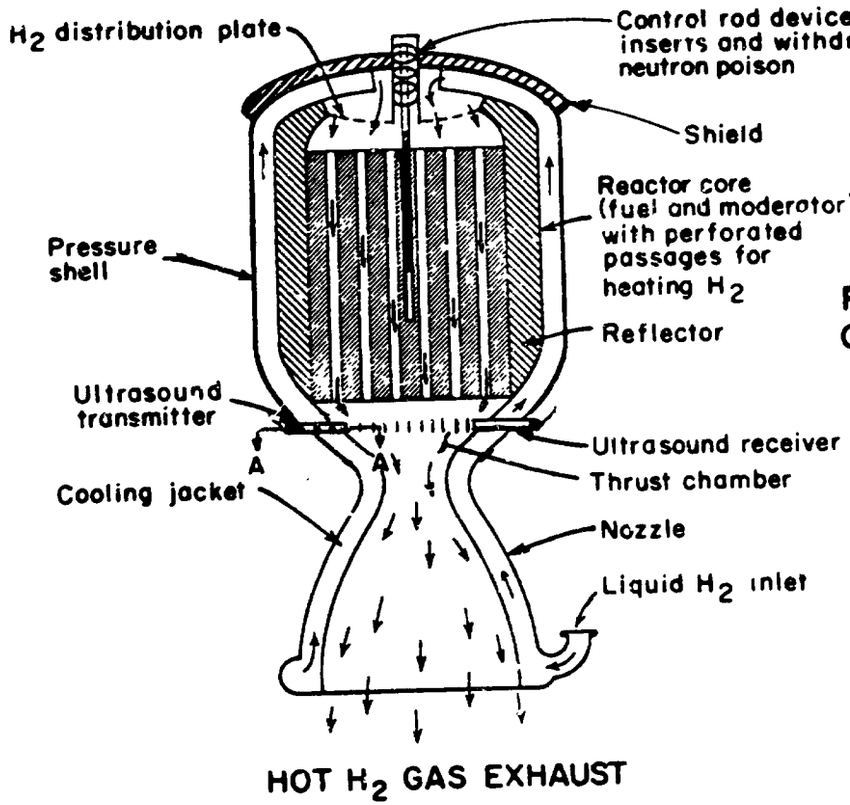

Figure 1a. Schematic diagram of fission reactor for nuclear rocket shows measurement location of ultrasonic temperature sensor (diagram adapted in part from Sutton[16], p. 390).

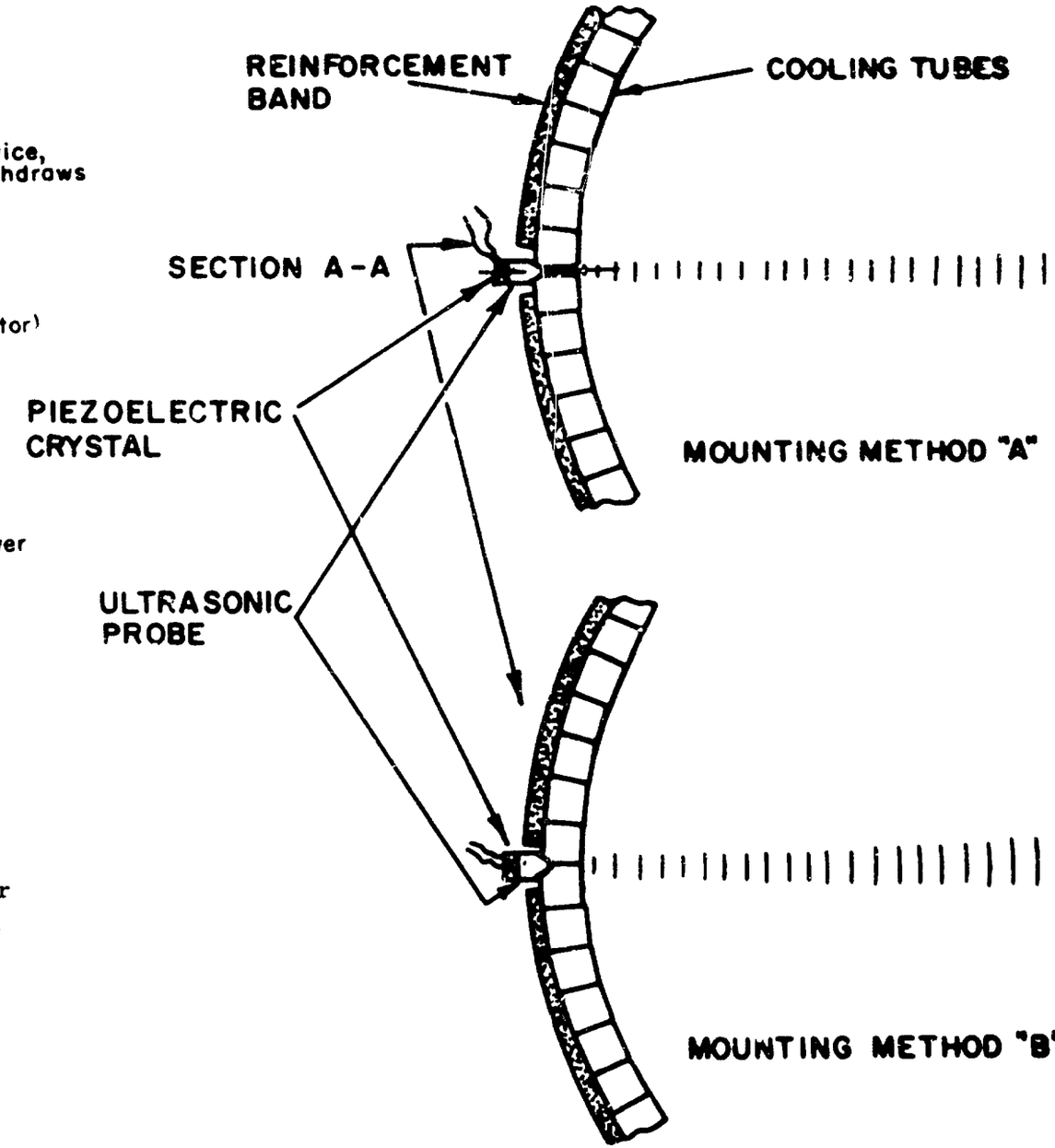

Figure 1b. Mounting methods. Mounting method "A" employs concept of inserting ultrasonic sensing probe between cooling tubes of thrust chamber, thereby allowing probe to protrude into the interior of thrust chamber. Mounting method "B" employs concept of mounting probe on exterior of thrust chamber, but in intimate contact with cooling tubes or reinforcement band.

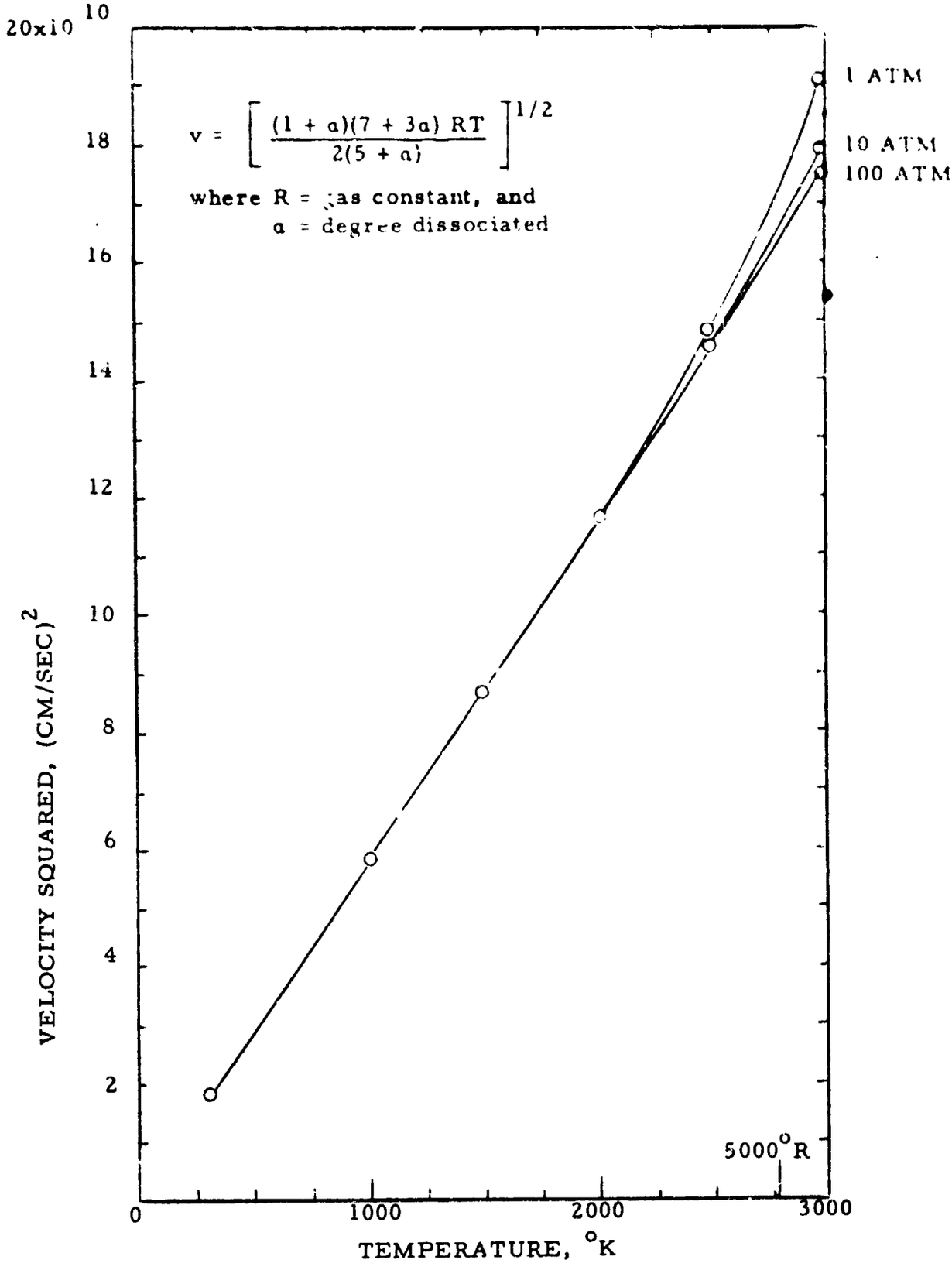

Figure 2. VELOCITY SQUARED VS. TEMPERATURE IN HYDROGEN

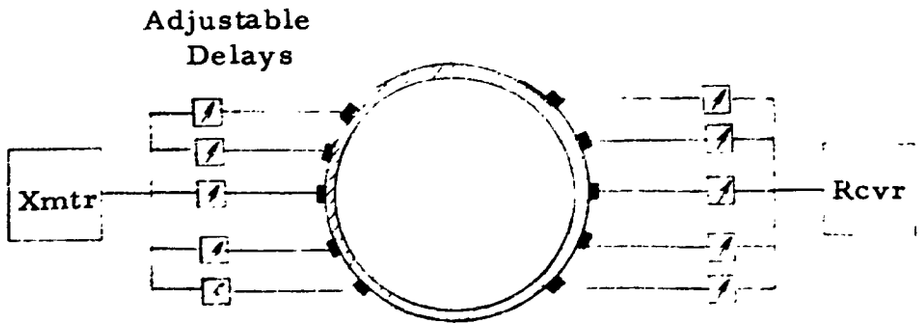

Figure 3a. Extended array of phased transducers.

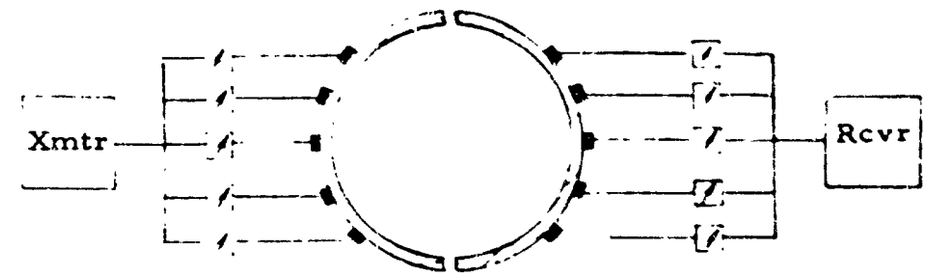

Figure 3b. Schematic of room temperature tests through air, using split thrust chamber to avoid acoustic short circuit.

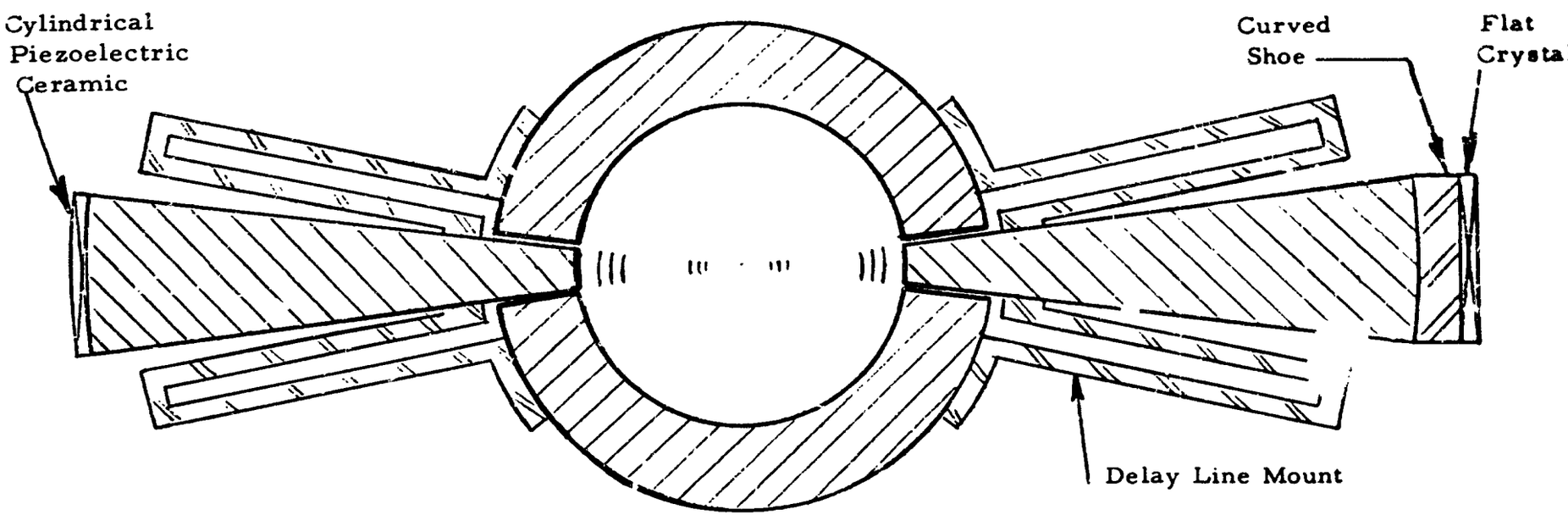

Figure 3c. Schematic of focussed transducers mounted on hydrogen/oxygen rocket engine.

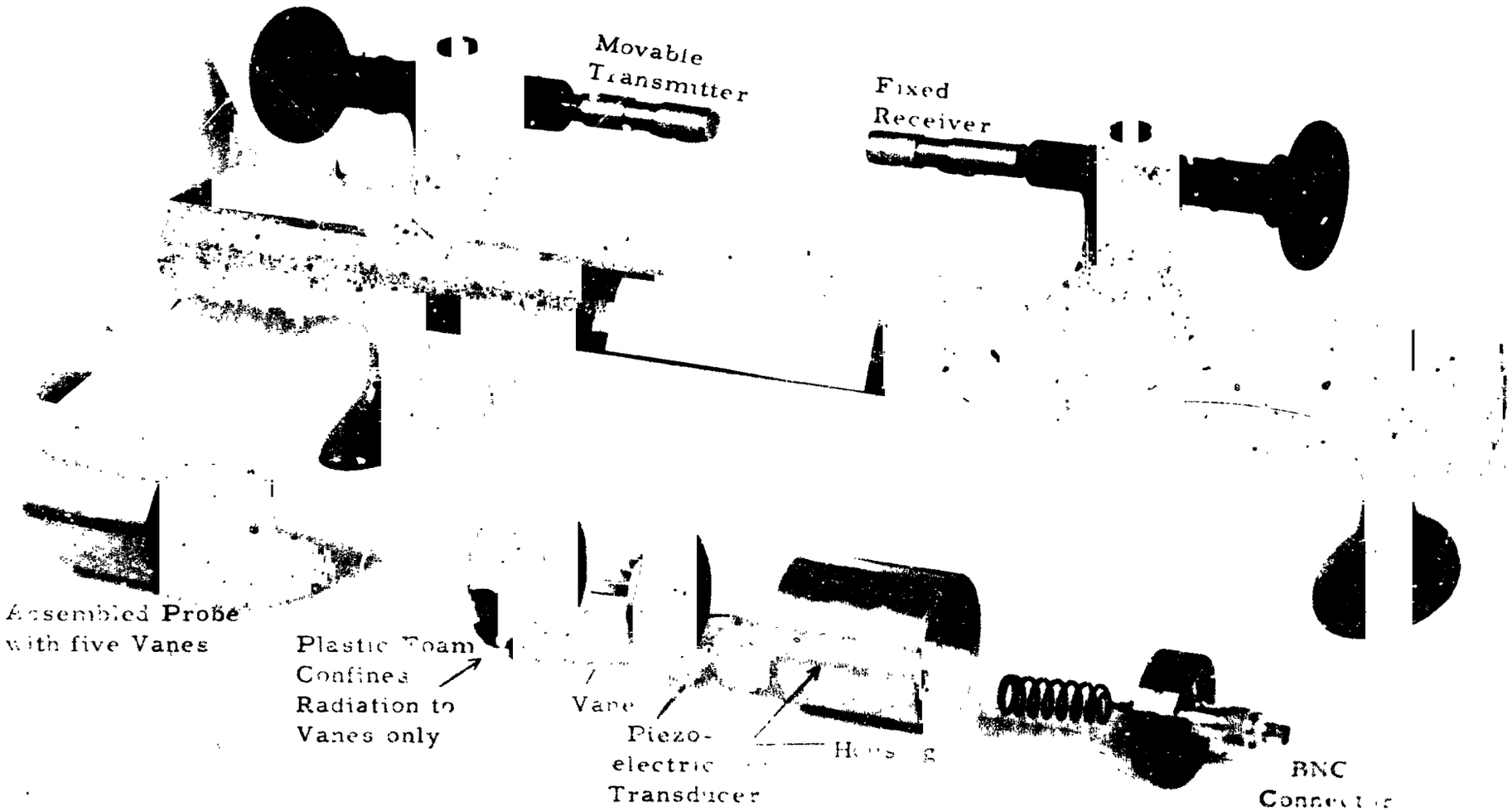

Figure 4. **Above,** variable air path yields same transit times as 2 ft hydrogen path at temperatures **indicated. Below, assembly and exploded views of a prototype vane probe.**

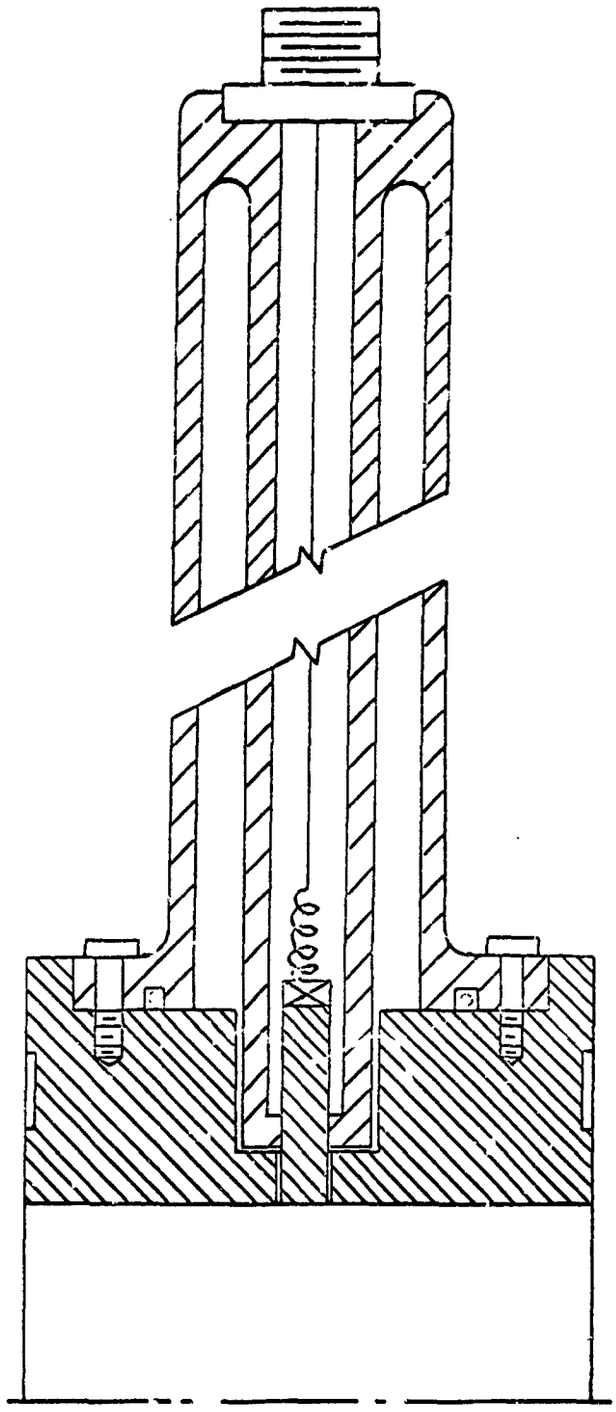

Figure 5. Schematic of ultrasonic sensor mount, using delay line between transducer and hydrogen/oxygen rocket engine test chamber.

Figure 6a. Assembly view of standard tubing and fittings, connected together in early model to demonstrate tubular delay line mounting concept. Air path = 2 inches (not shown).

Figure 6b. Exploded view.

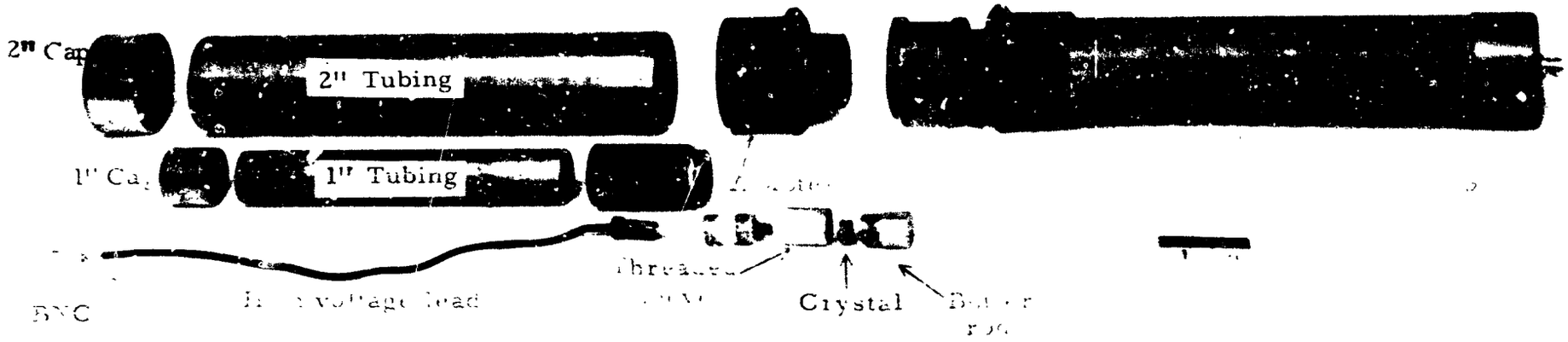

Figure 6c. Assembly view of first water [illegible] mounts used in hydrogen/oxygen rocket engine tests, August 1965.

Figure 6d. Exploded view.

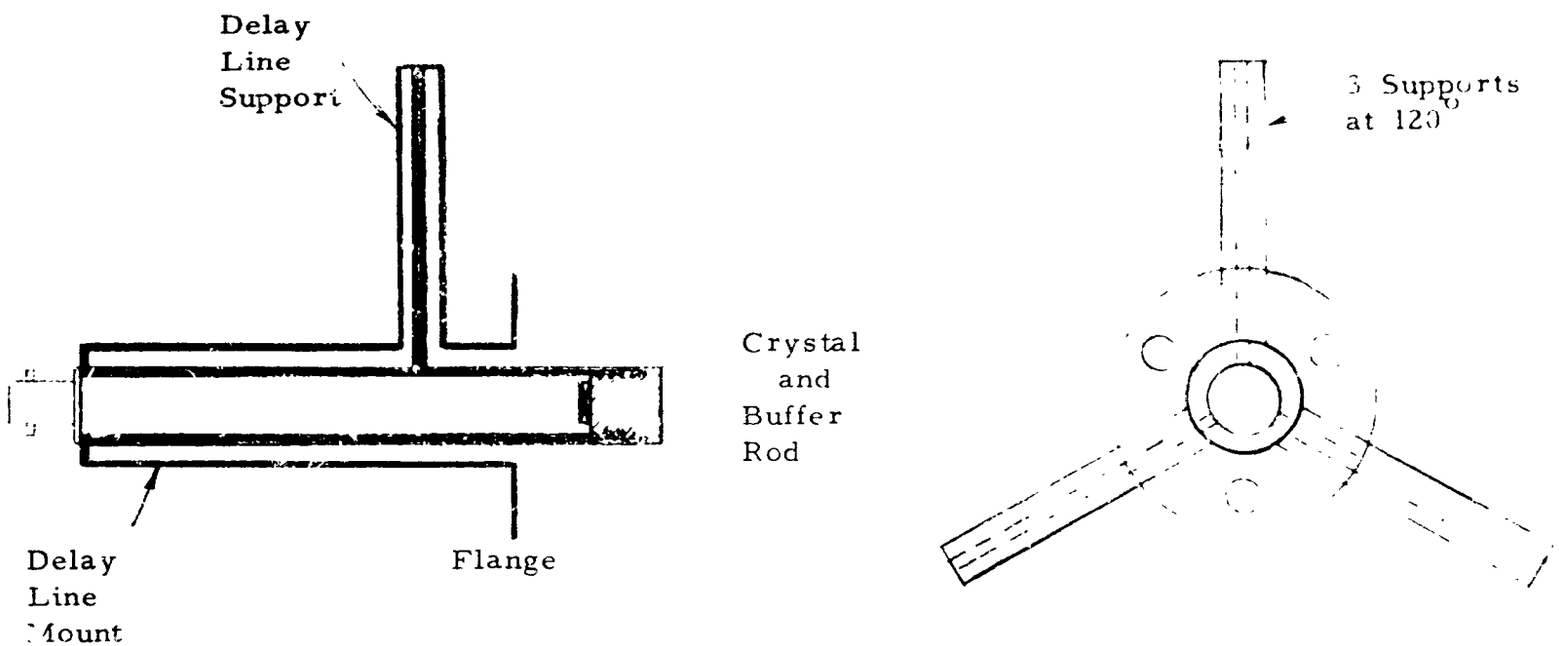

Figure 7. Reinforced cantilever delay line mount.

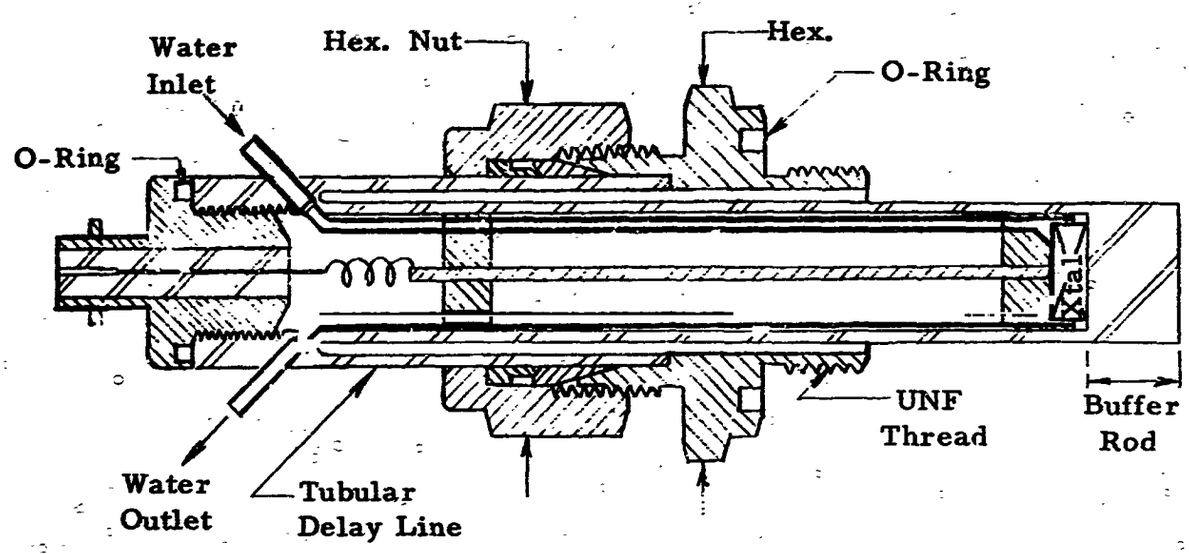

Figure 8a. Delay line mount utilizing standard high pressure fittings.

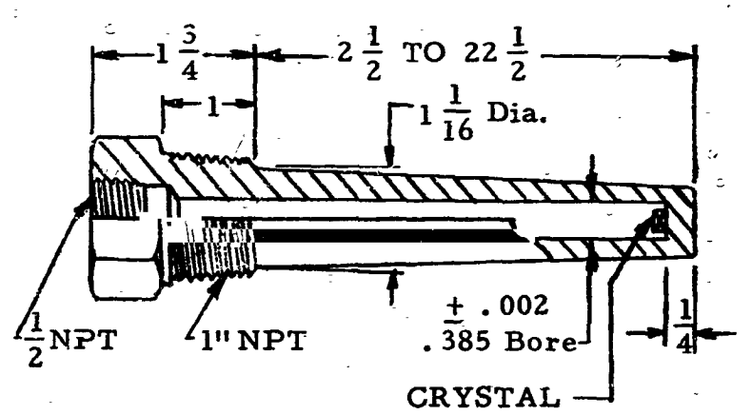

Figure 8b. Delay line mount utilizing standard thermowell. (Electrical connections, water cooling not shown).

Figure 9. Coiled tube gives ~1 ms delay

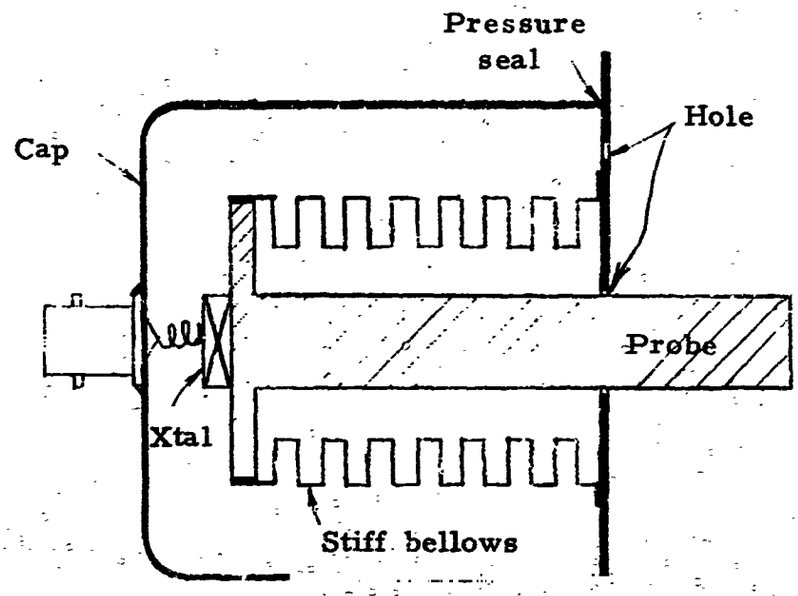

Figure 10. Bellows mount.

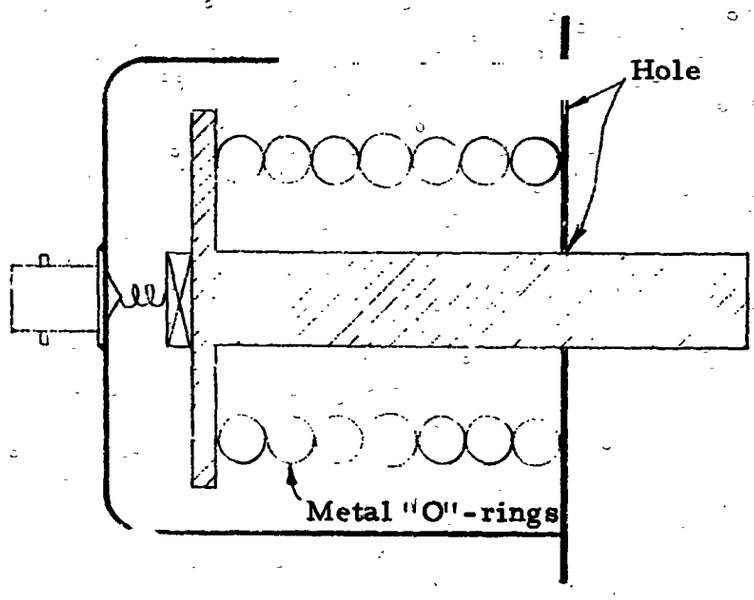

Figure 11. Metal "O"-ring mount.

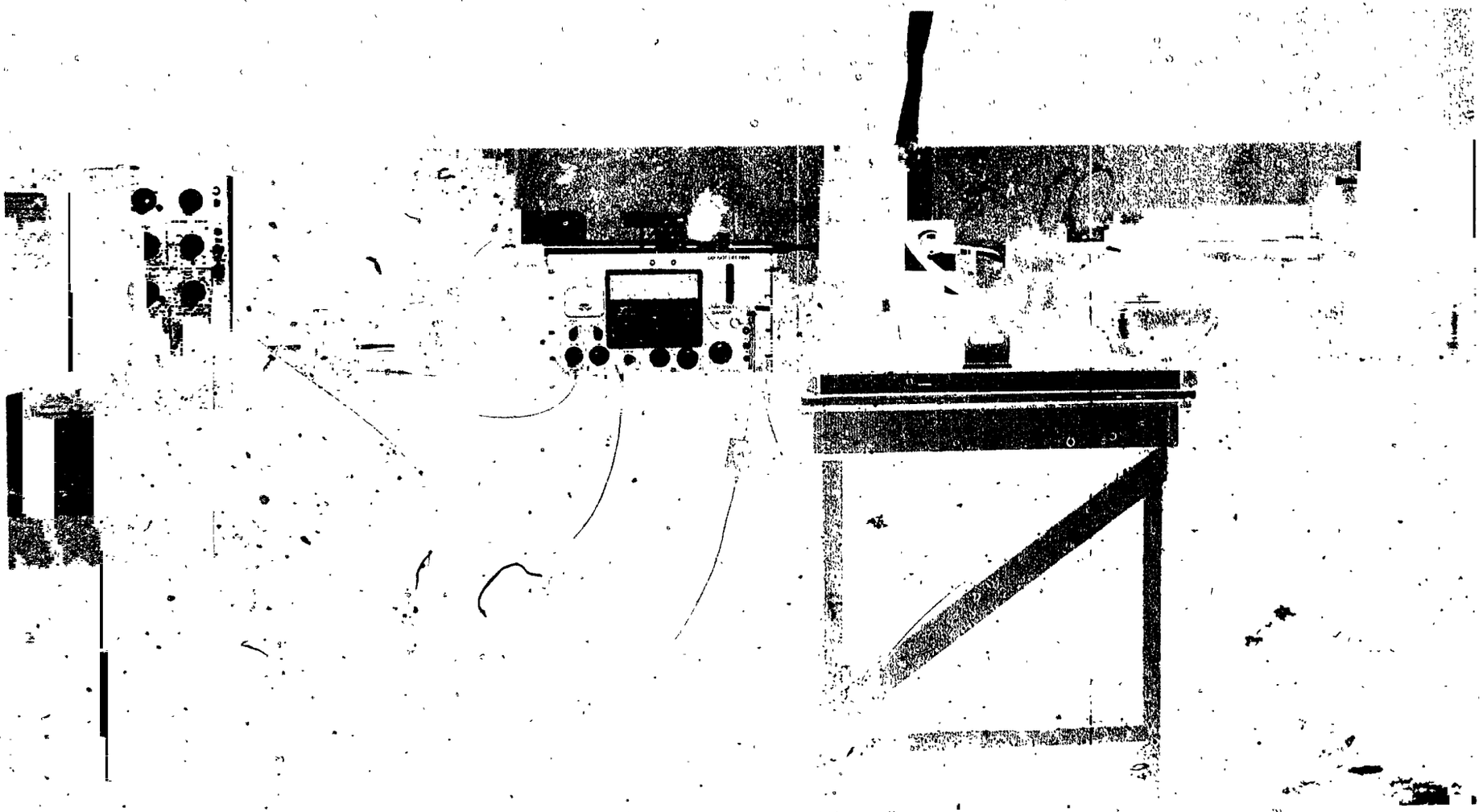

Figure 12. Pneumatically actuated probes for momentary contact gas diagnostics.

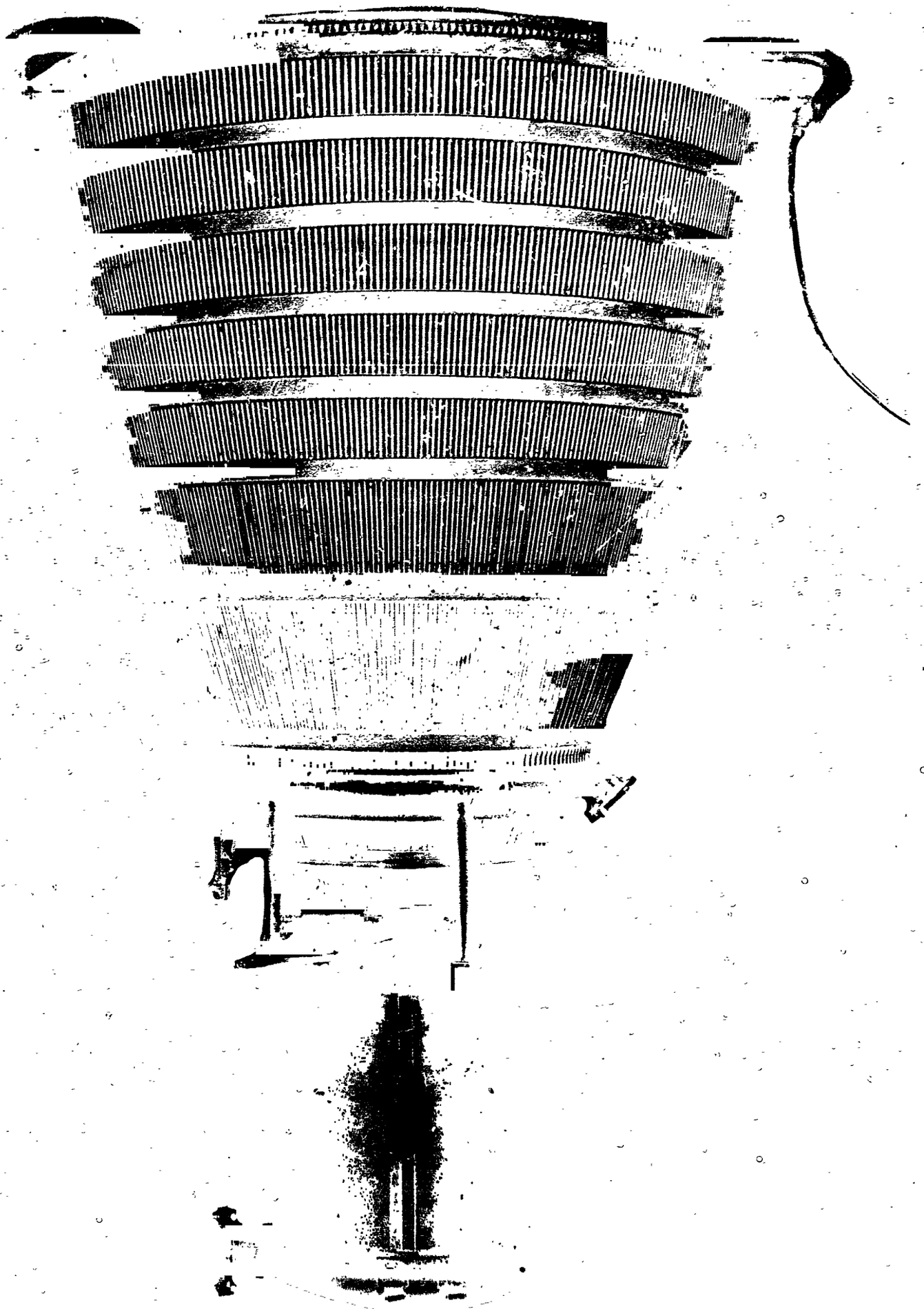

Figure 13. - Centaur thrust chamber for studying acoustic short circuit.

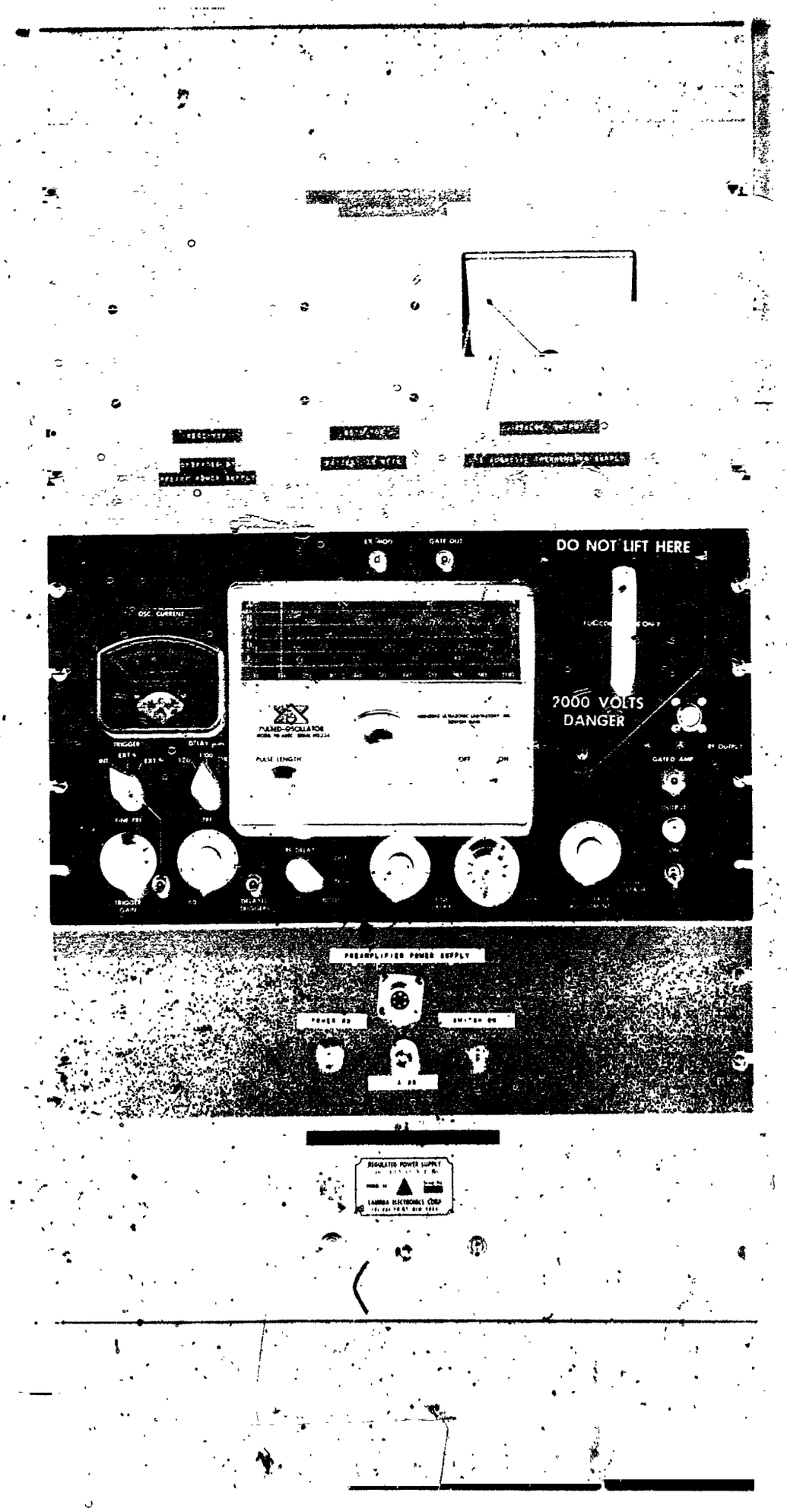

Figure 14. Instrumentation for ultrasonic gas temperature measurement

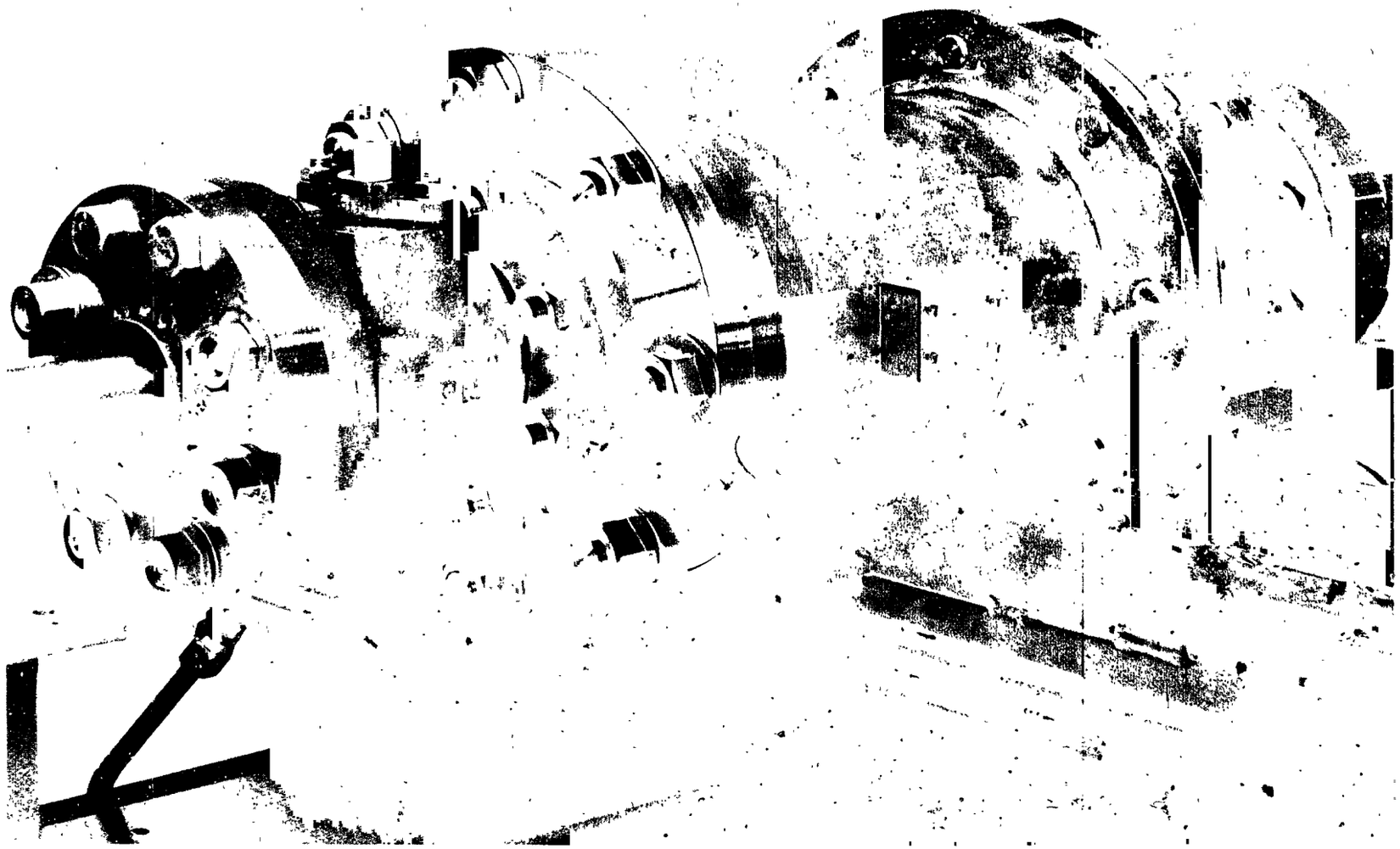

Figure 15. Muffle tube oven

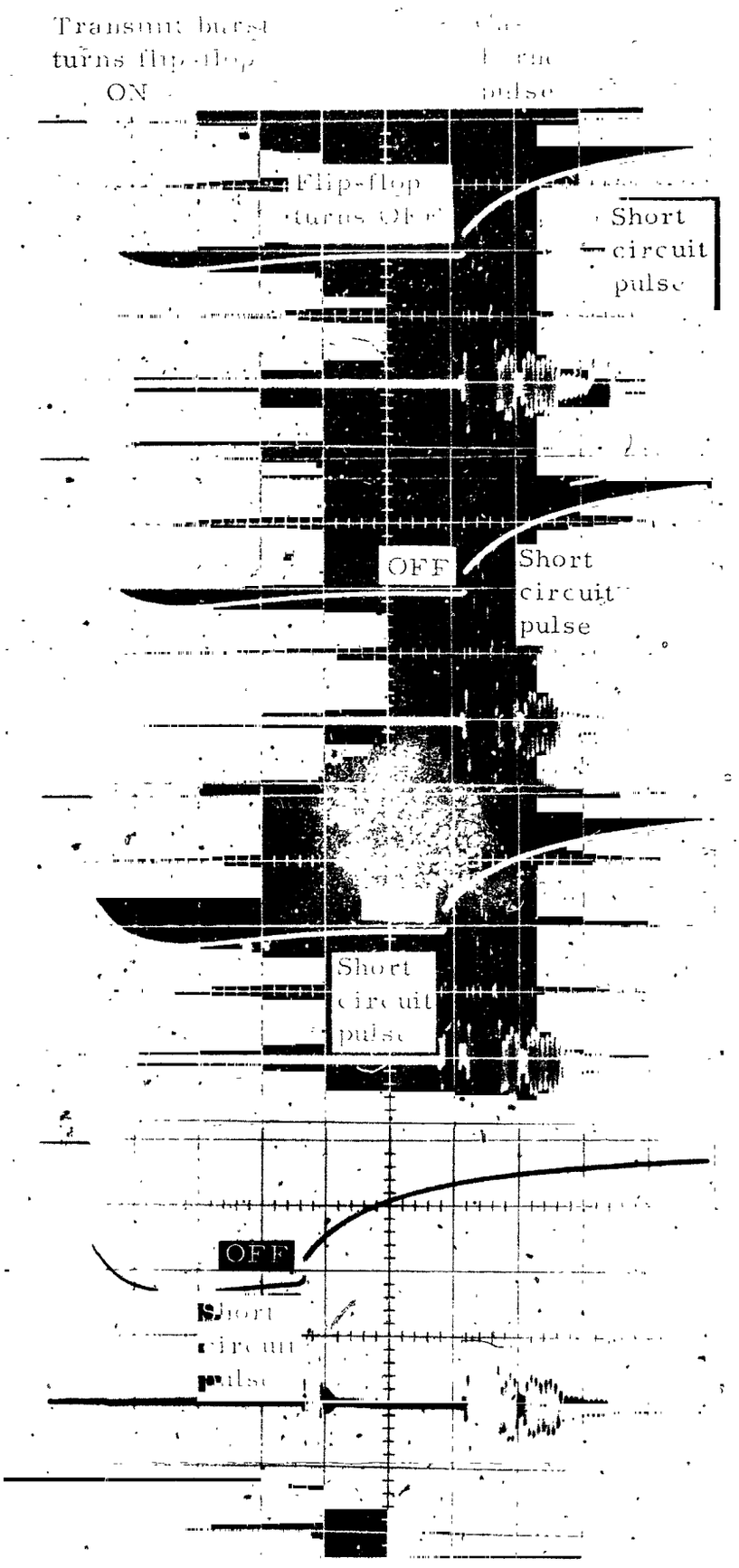

Upper trace: flip-flop output to transit time integrator.

Lower trace: superposition of gas borne and short circuit pulses.

No degradation despite short circuit pulse immediately after gas borne pulse.

Two examples show that when short circuit pulse is artificially injected early, it turns flip-flop OFF too soon.

Figure 1[illegible] Oscilloscope [illegible] demonstrate electrical performance of [illegible] circuitry. Waveform sequence shows no [illegible] acoustic short circuit, for simulated [illegible] temperatures of 1000 to 5000°R.

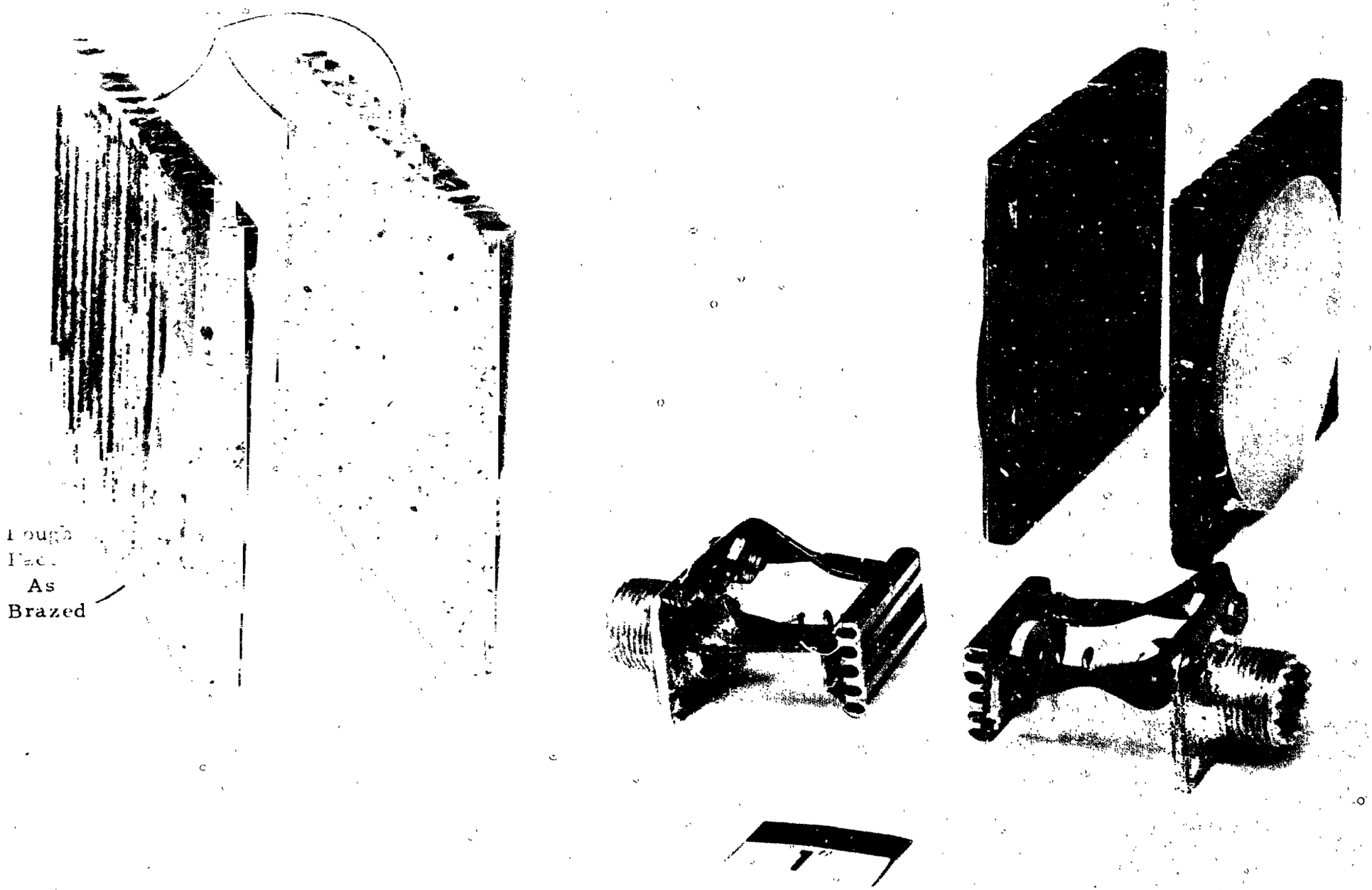

Figure 17. Brazed test panels.

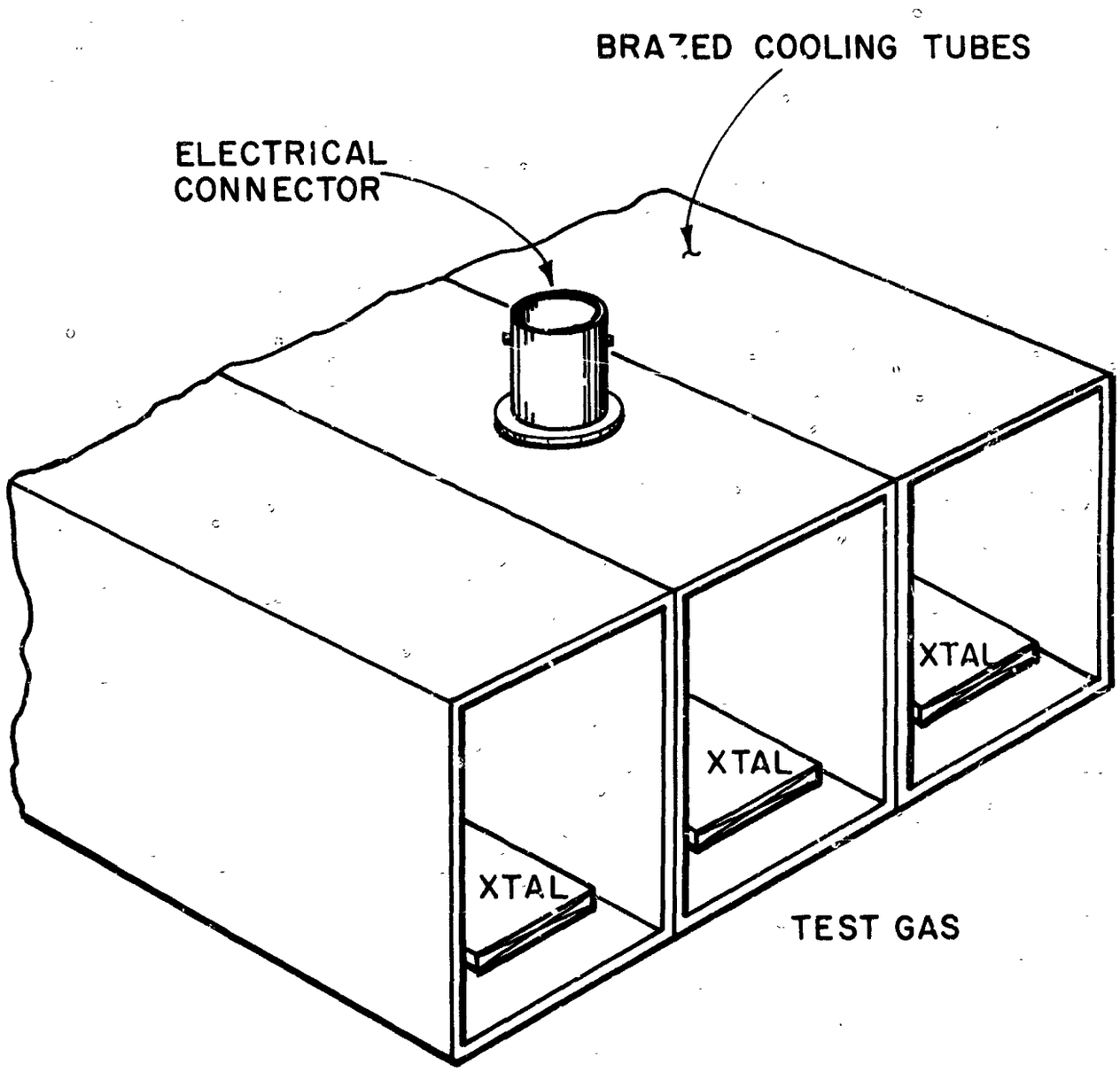

Figure 18. Crystals inside cooling tubes yield increased ultrasonic transmission into test gas.

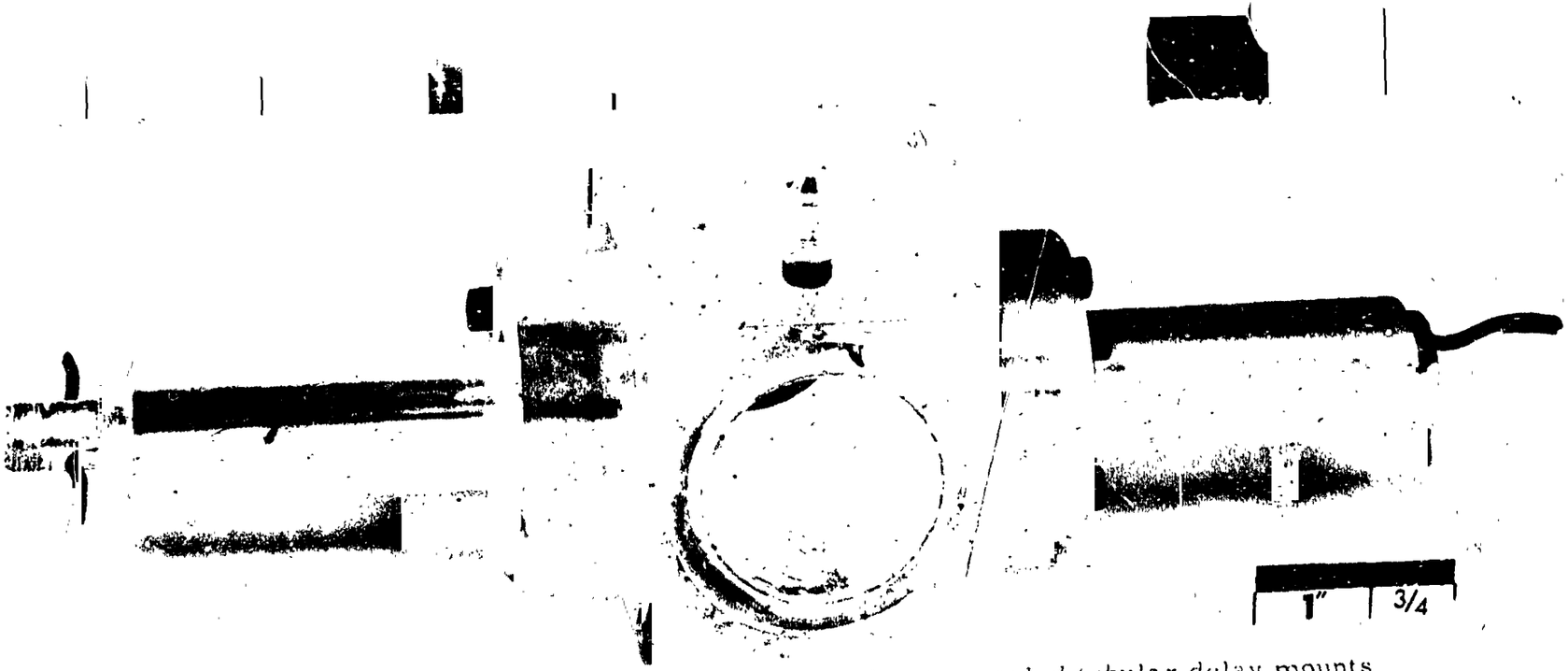

Figure 19a. Assembly view of second pair of water cooled tubular delay mounts used in hydrogen/oxygen rocket engine tests, August 1965.

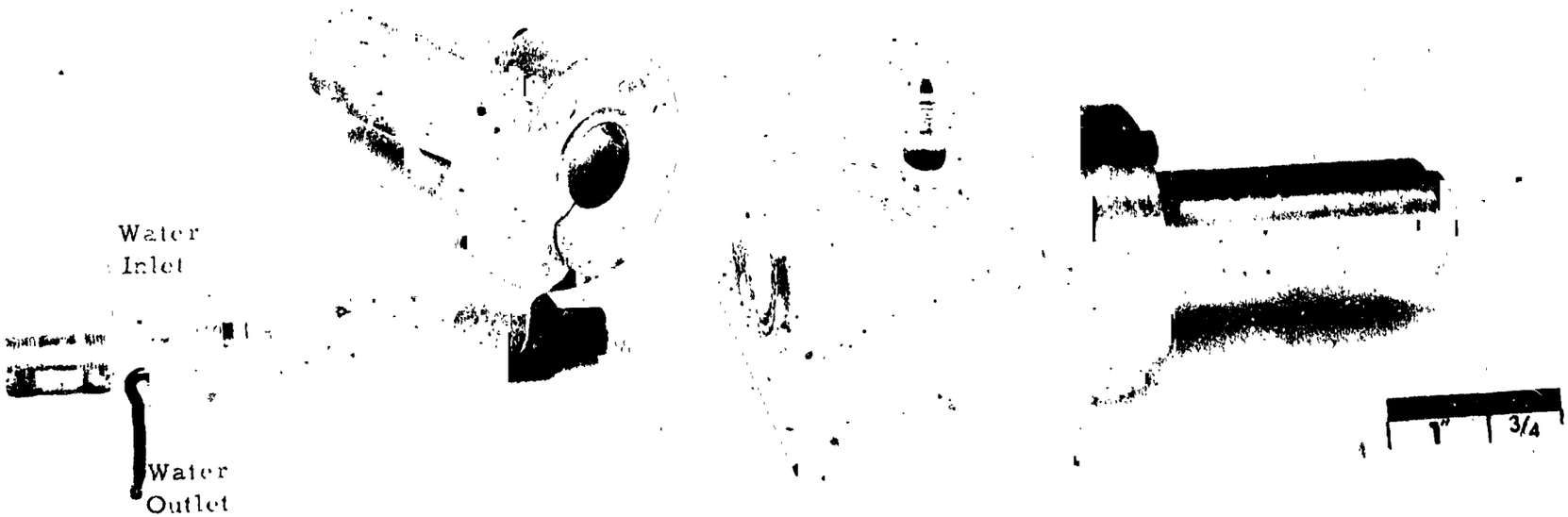

Figure 19b. Exploded view, showing adjustable probe mounts for hydrogen/oxygen rocket engine studies.

Figure 20. Thick walled copper test

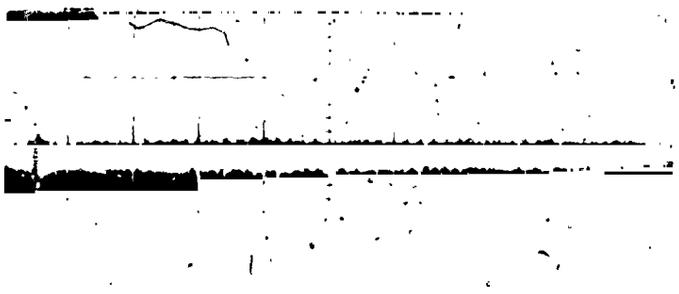

Upstream noise during ignition
12 Aug 65 50 μs/cm

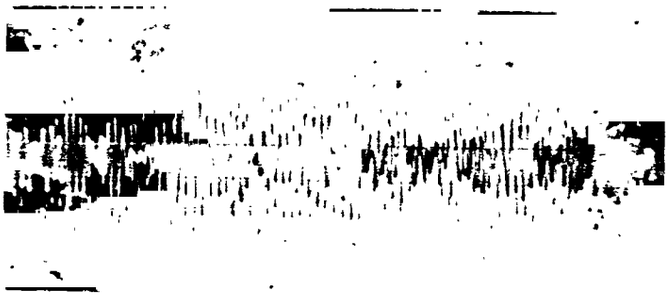

Upstream noise during combustion
13 Aug 65 20 μs/cm

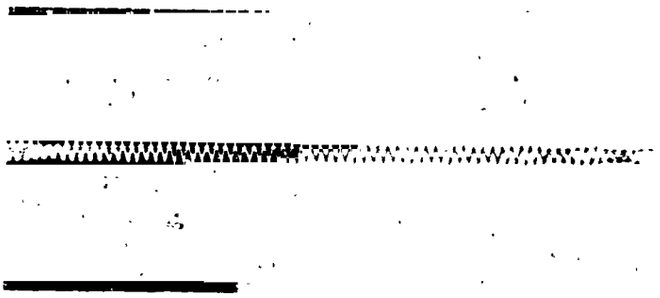

Downstream noise during combustion
13 Aug 65 20 μs/cm

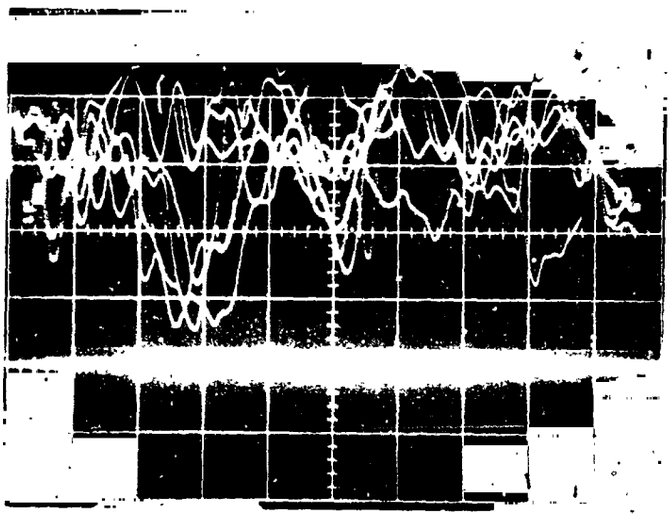

Upstream noise during combustion.
Top: Wideband receiving system.
Bottom: Bliley narrow band filter, f_0 500 kHz in receiver circuit.
12 Aug 65 20 μs/cm

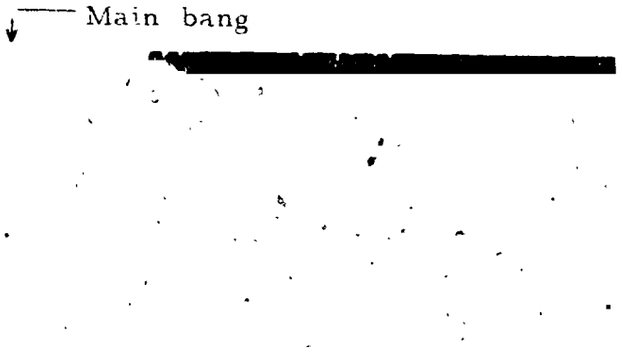

Downstream noise (left portion of trace) plus possible signal (right portion of trace) during combustion.
13 Aug 65 20 μs/cm

Figure 21. Typical waveforms observed during ignition and combustion tests at NASA-Lewis in August 1965.

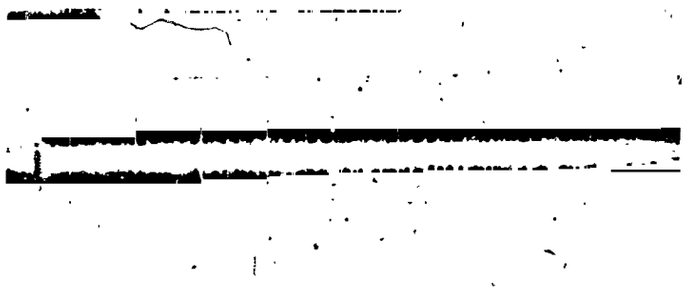

Upstream noise during ignition
12 Aug 65 50 μs/cm

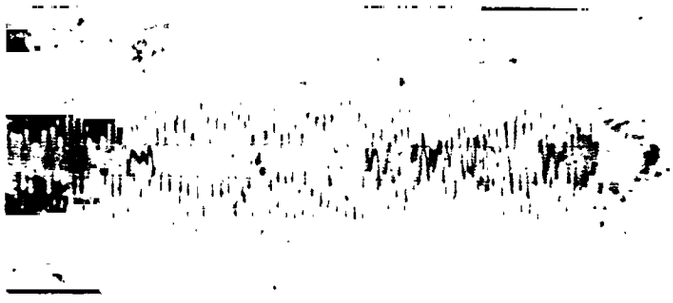

Upstream noise during combustion
13 Aug 65 20 μs/cm

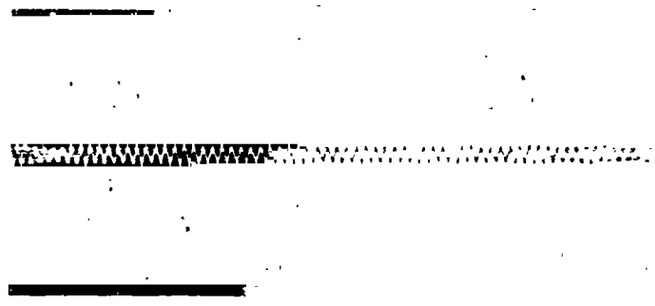

Downstream noise during combustion
13 Aug 65 20 μs/cm

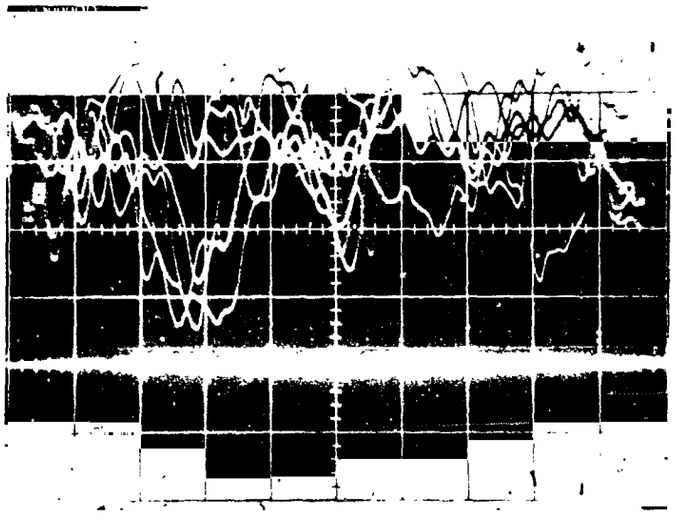

Upstream noise during combustion.
Top: Wideband receiving system.
Bottom: Bliley narrow band filter, f_o = 500 kHz in receiver circuit.
12 Aug 65 20 μs/cm

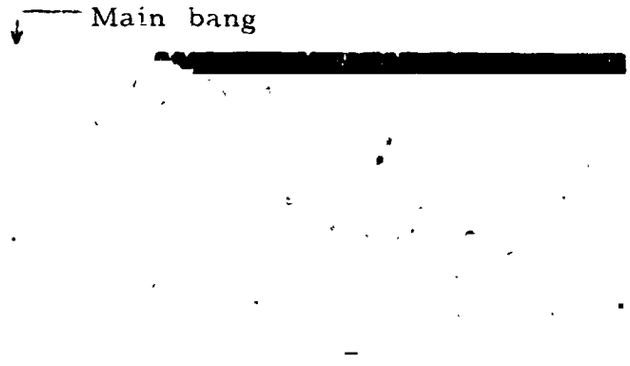

Downstream noise (left portion of trace) plus possible signal (right portion of trace) during combustion.
13 Aug 65 20 μs/cm

Figure 21. Typical waveforms observed during ignition and combustion tests at NASA-Lewis in August 1965.

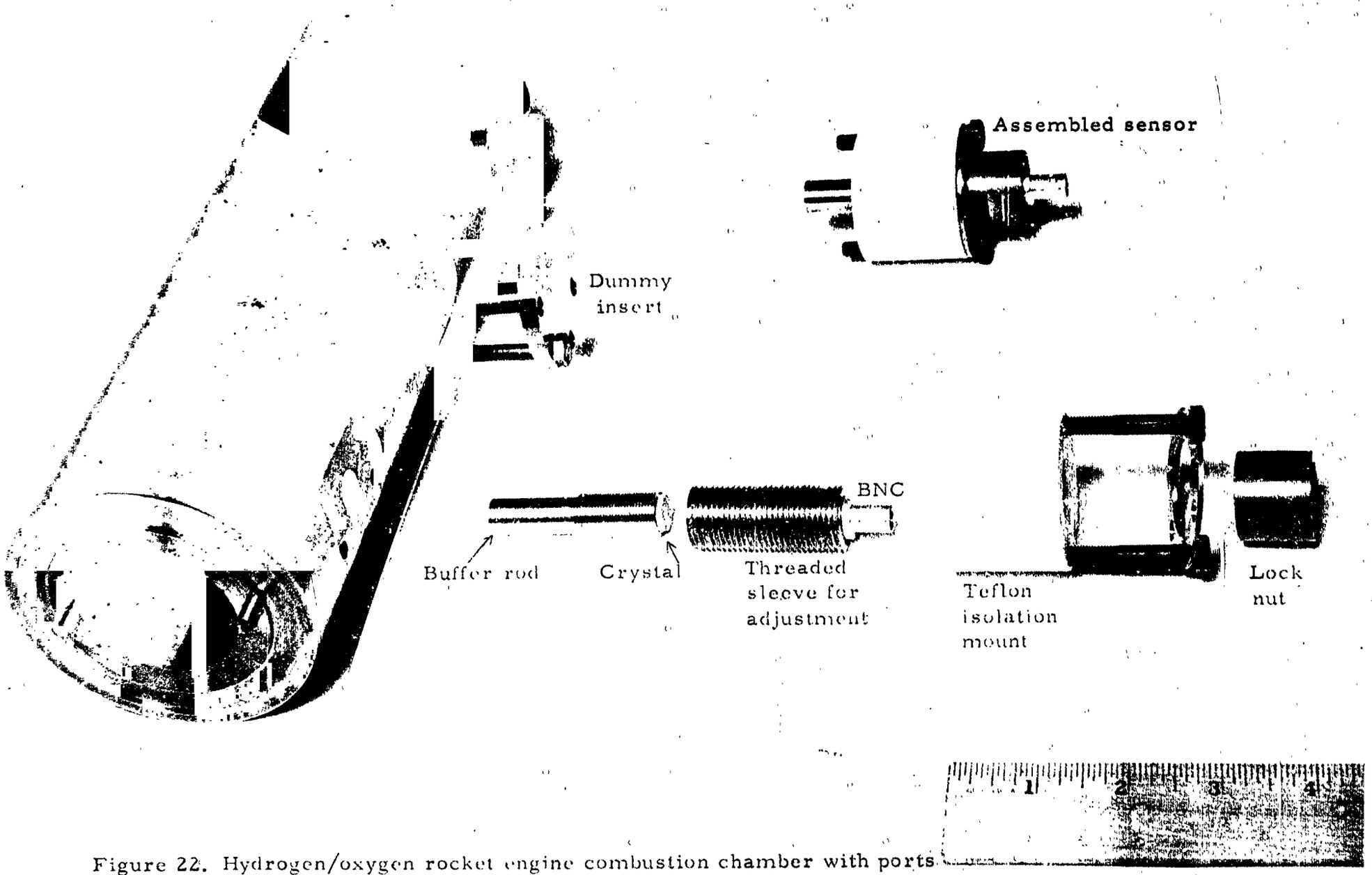

Figure 22. Hydrogen/oxygen rocket engine combustion chamber with ports for ultrasonic sensors. Adjustable, externally water cooled isolation mounts were used in second series of tests at NASA-Lewis, January 1966.

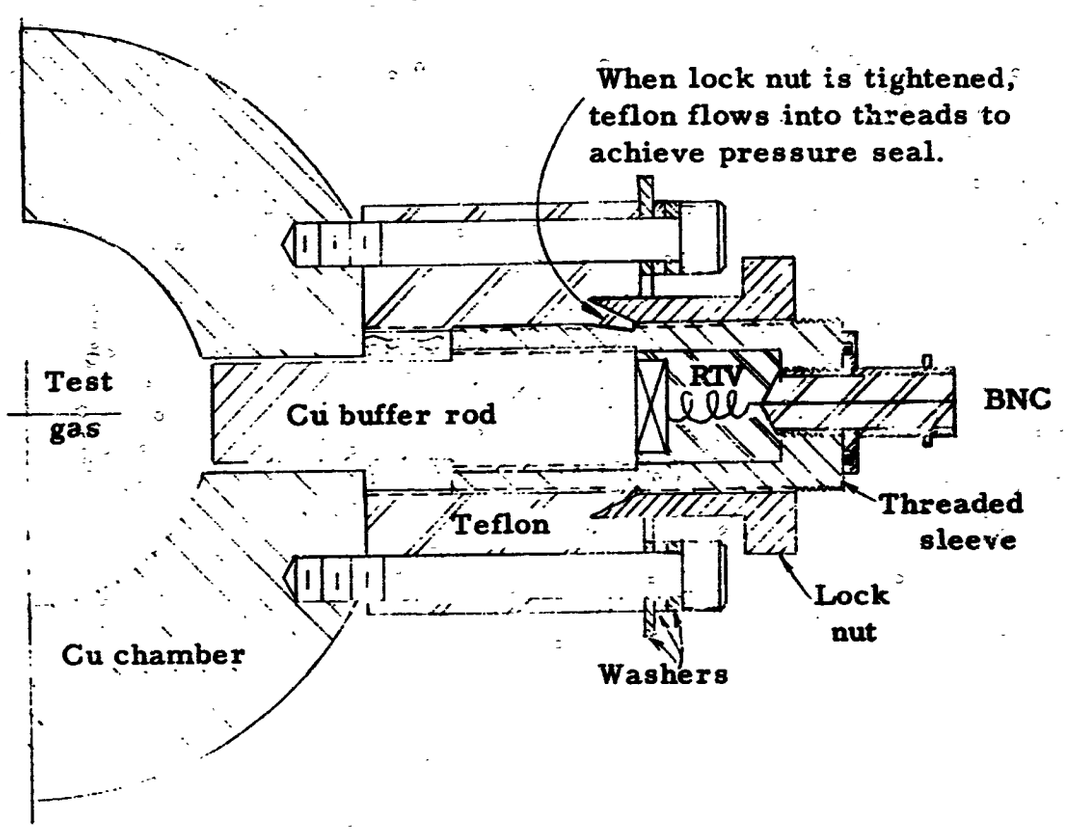

Figure 23. Teflon isolation mount.

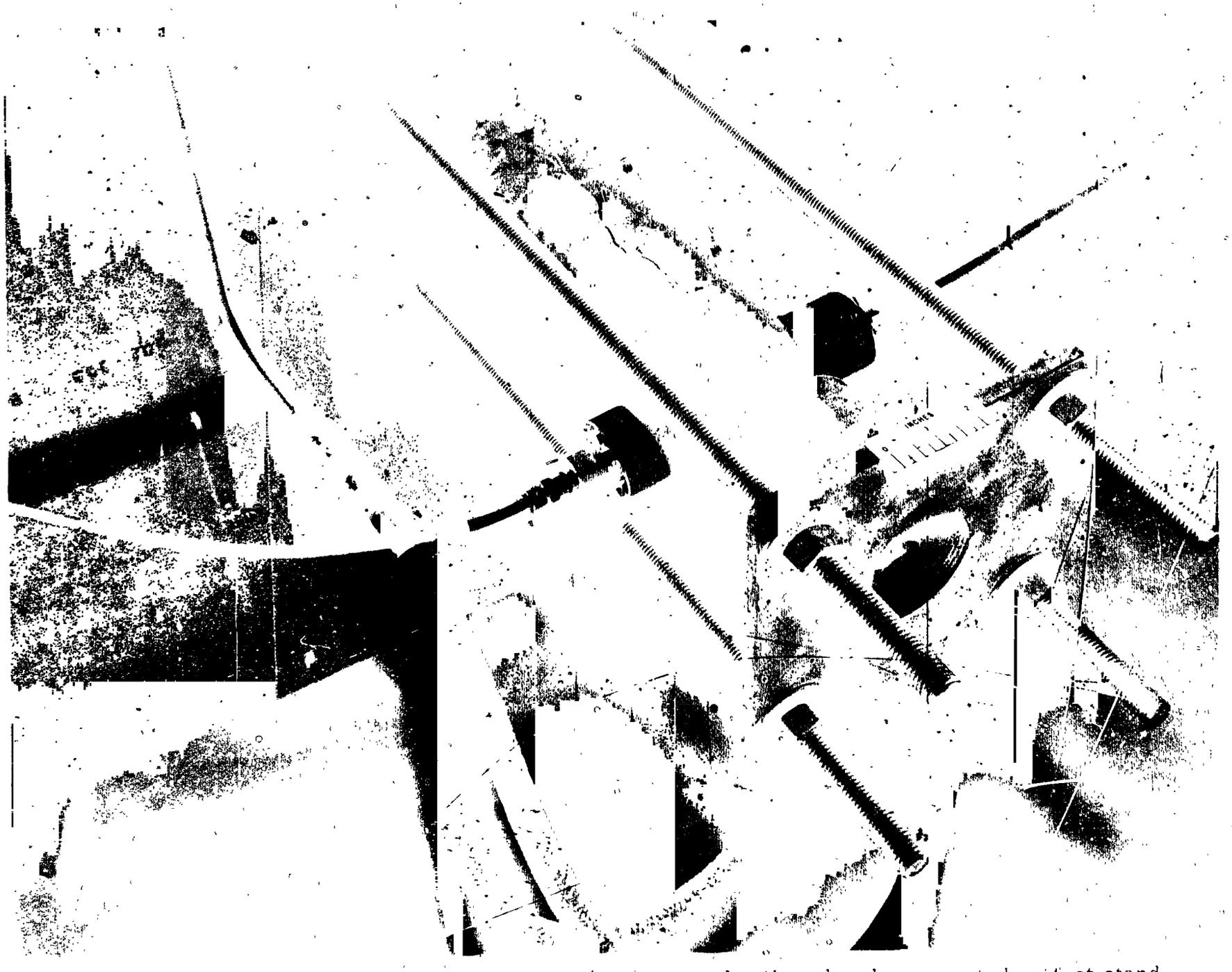

Figure 24. Hydrogen/oxygen combustion chamber mounted on test stand.

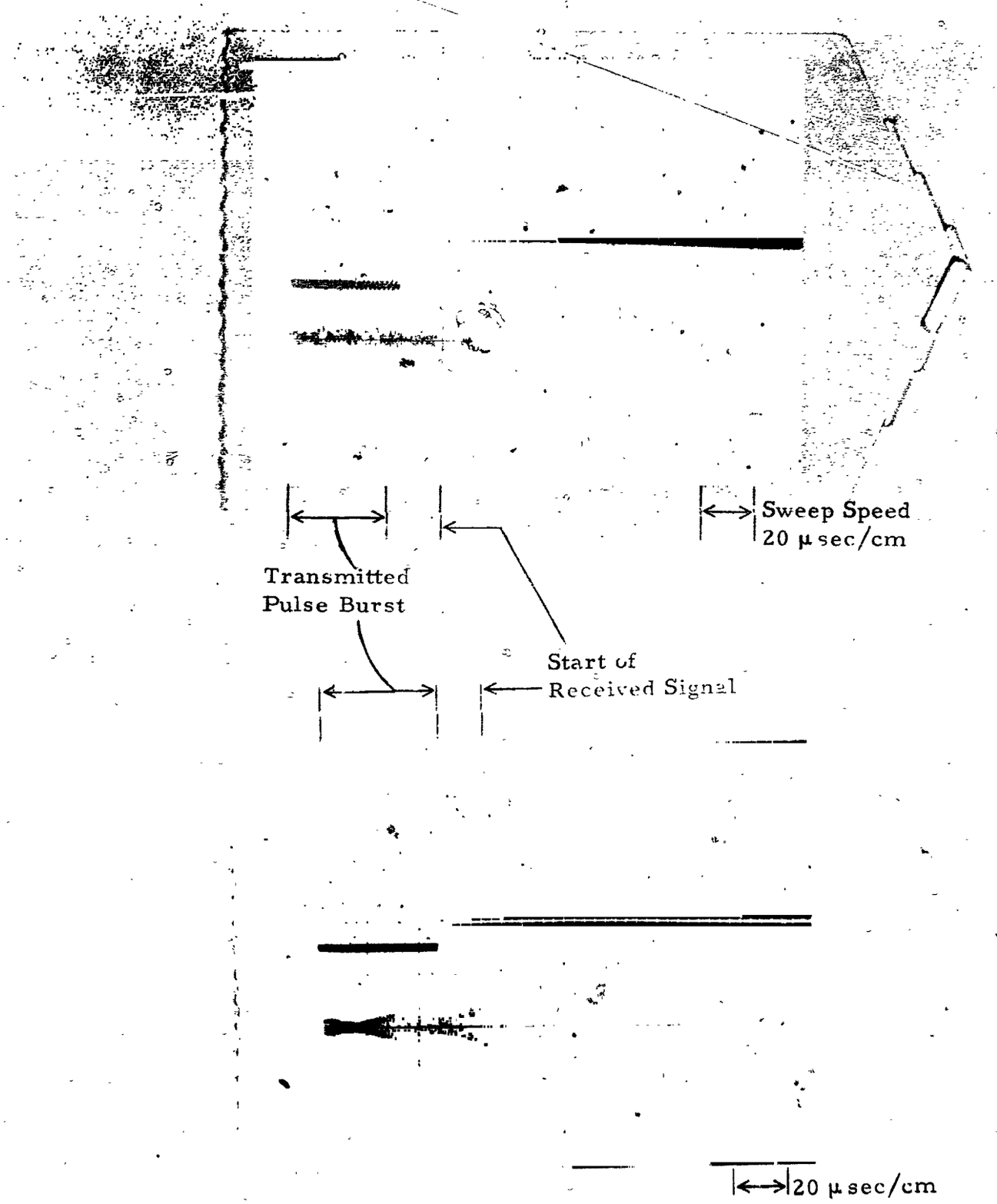

Figure 25. Measurement of ultrasonic pulses despite severe noise in hydrogen/oxygen rocket engine tests at NASA-Lewis in January 1966.

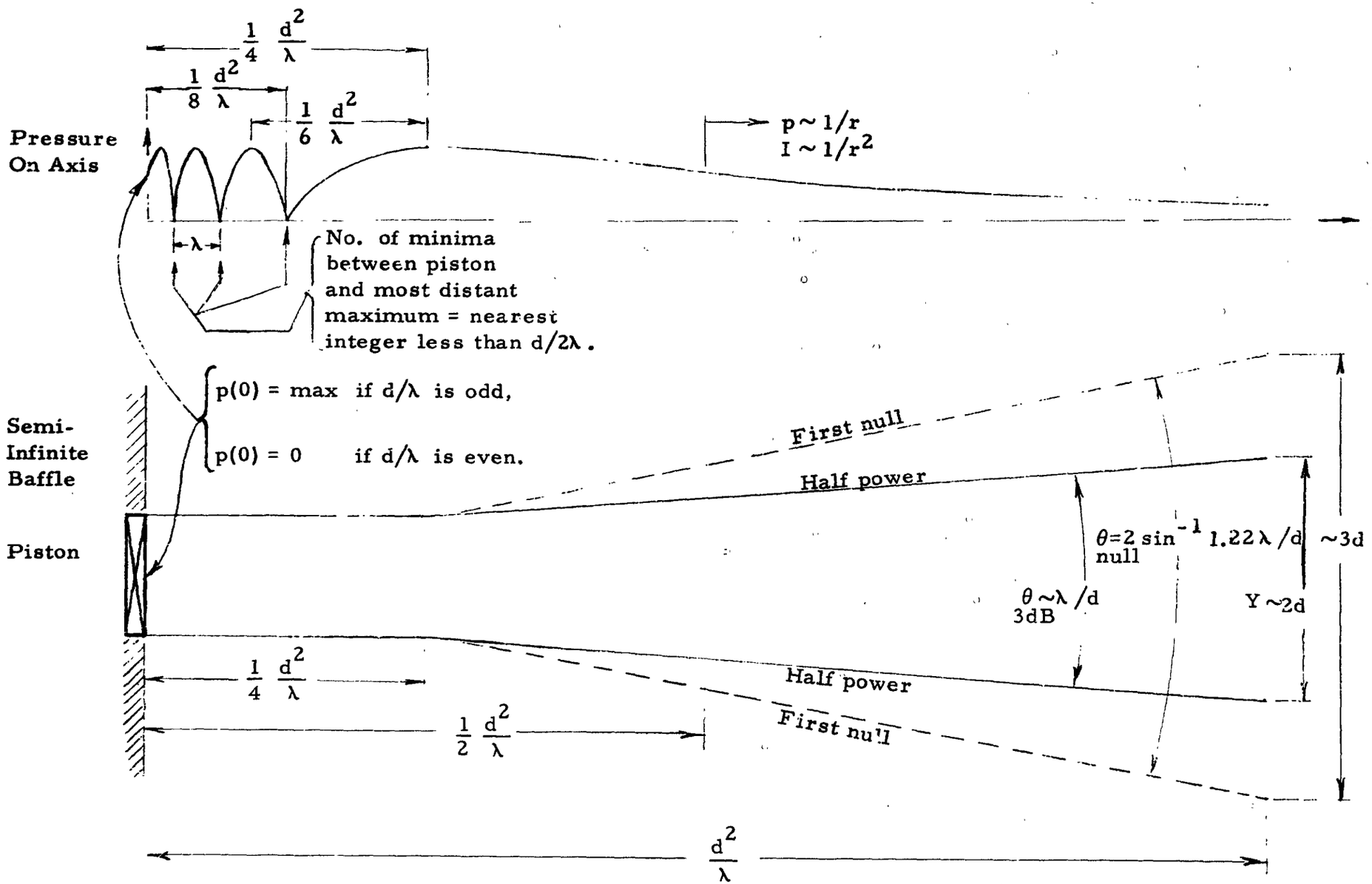

Figure 26. Beam characteristics of circular piston. Dimensions shown are approximations suitable for estimating purposes.

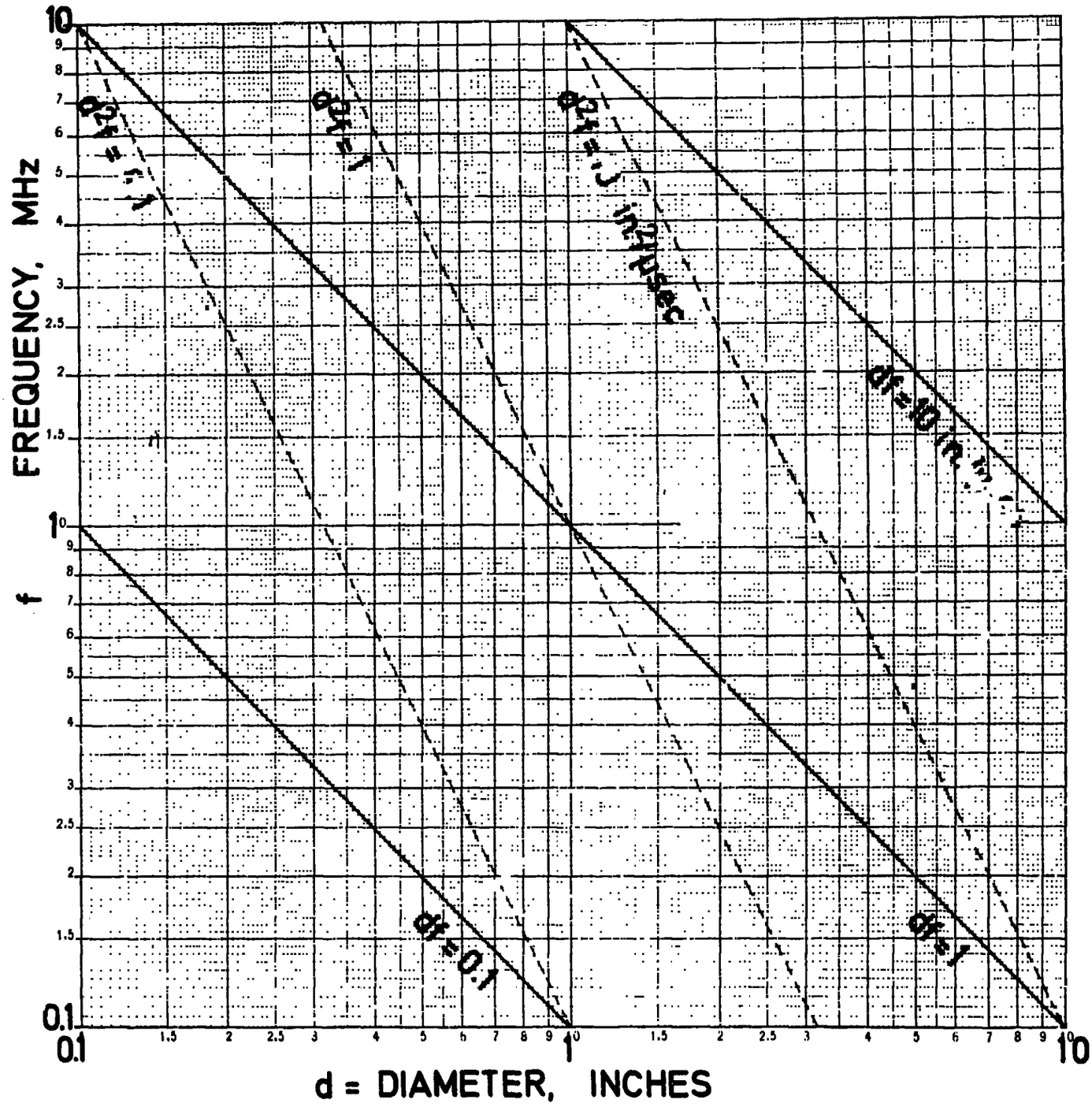

Figure 27. Frequency-diameter nomogram

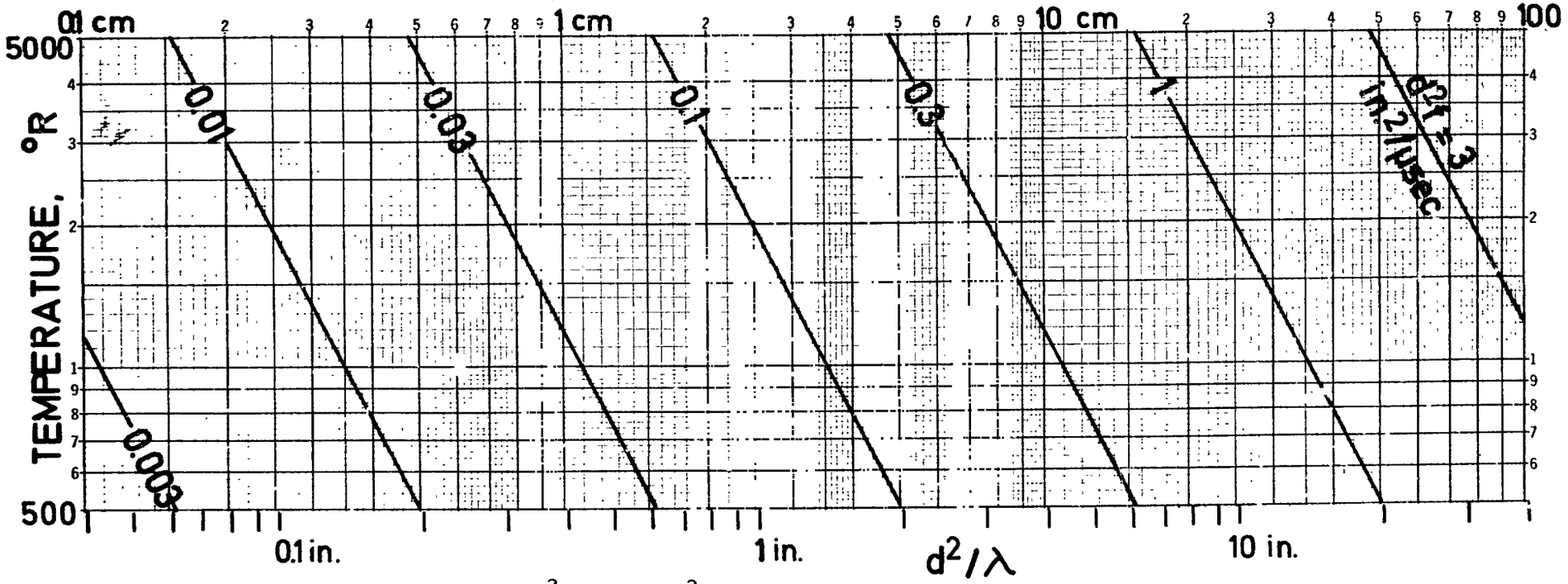

Figure 28. Temperature vs d^2/λ, with d^2f as parameter.

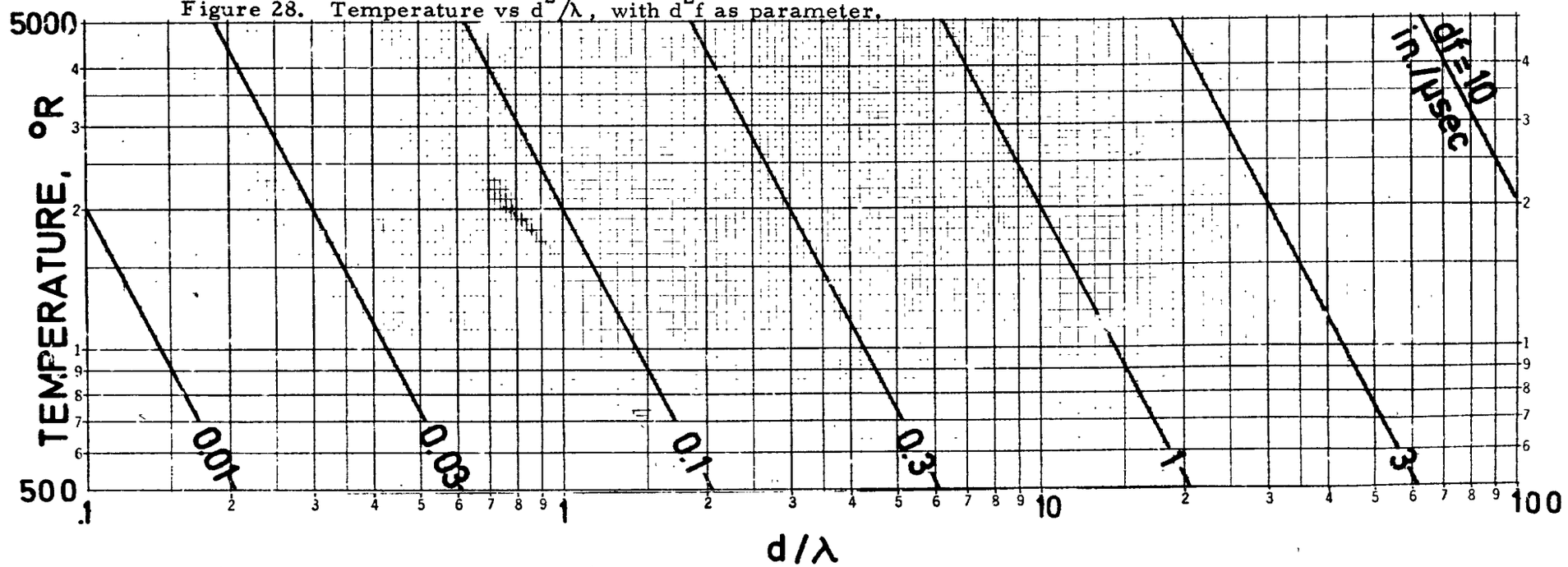

Figure 29. Temperature vs d/λ, with df as parameter.

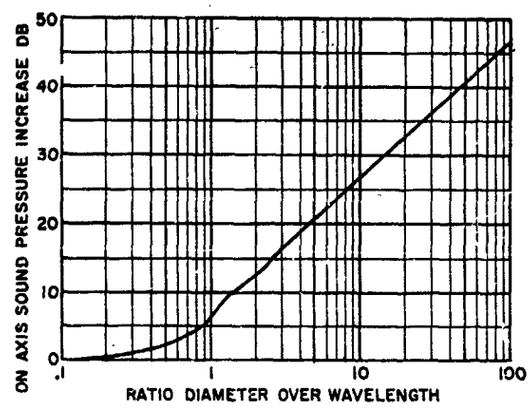

Figure 30. Increase in sound-pressure level along the normal axis of a piston generating constant acoustic power, as a function of the ratio of piston diameter to wavelength of sound, after Massa.[33]

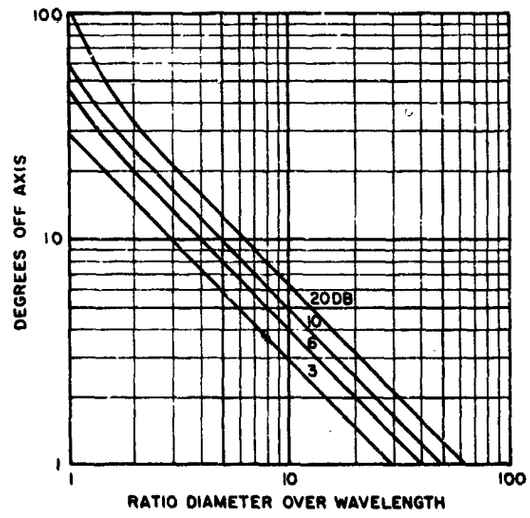

Figure 31. Directional radiation pattern from a vibrating circular piston, showing the degrees off the normal axis at which the attenuation is 3, 6, 10 and 20 dB, as a function of piston diameter over wavelength, after Massa.[33]

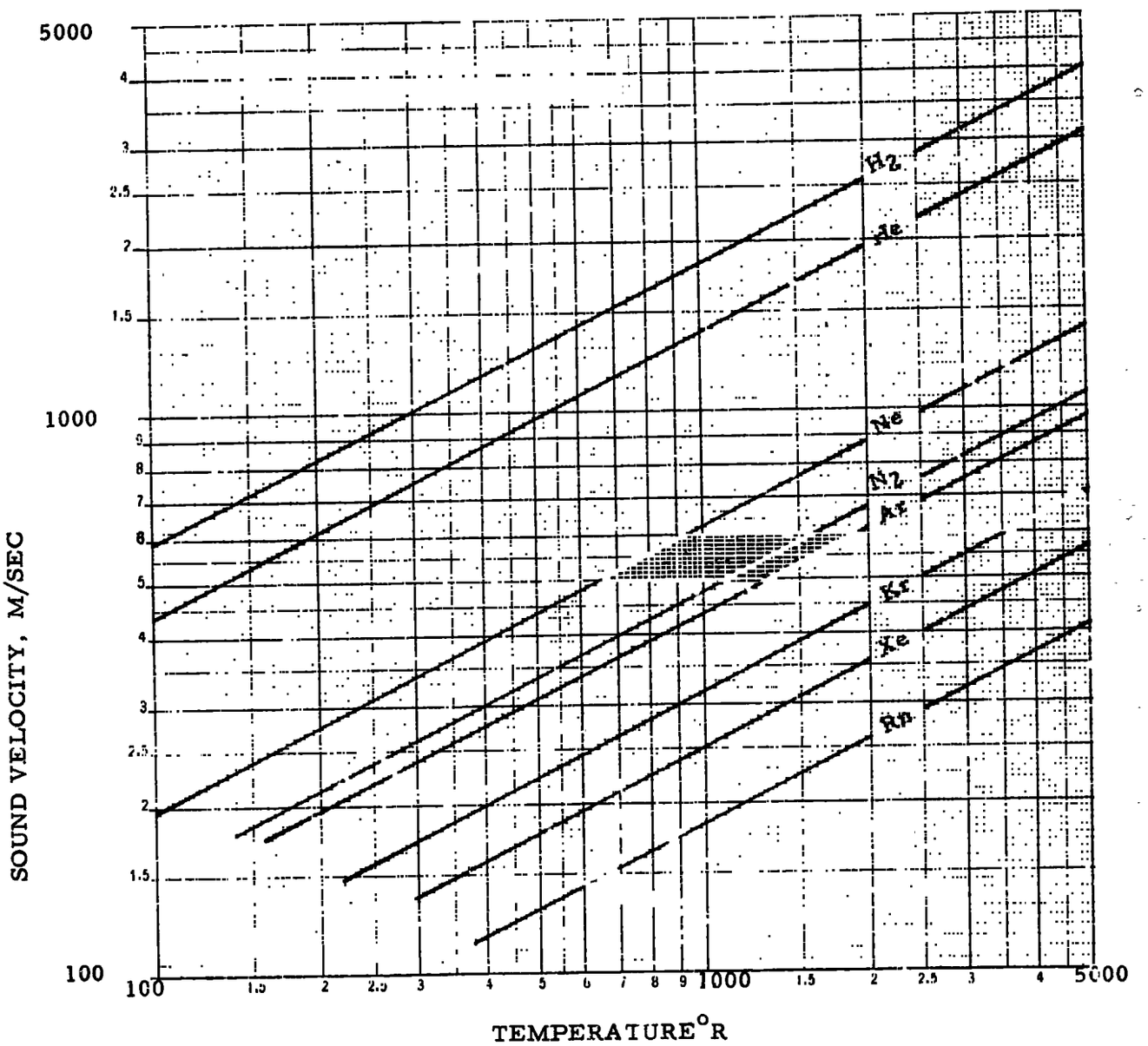

Figure 32. Sound velocity vs temperature in various gases.

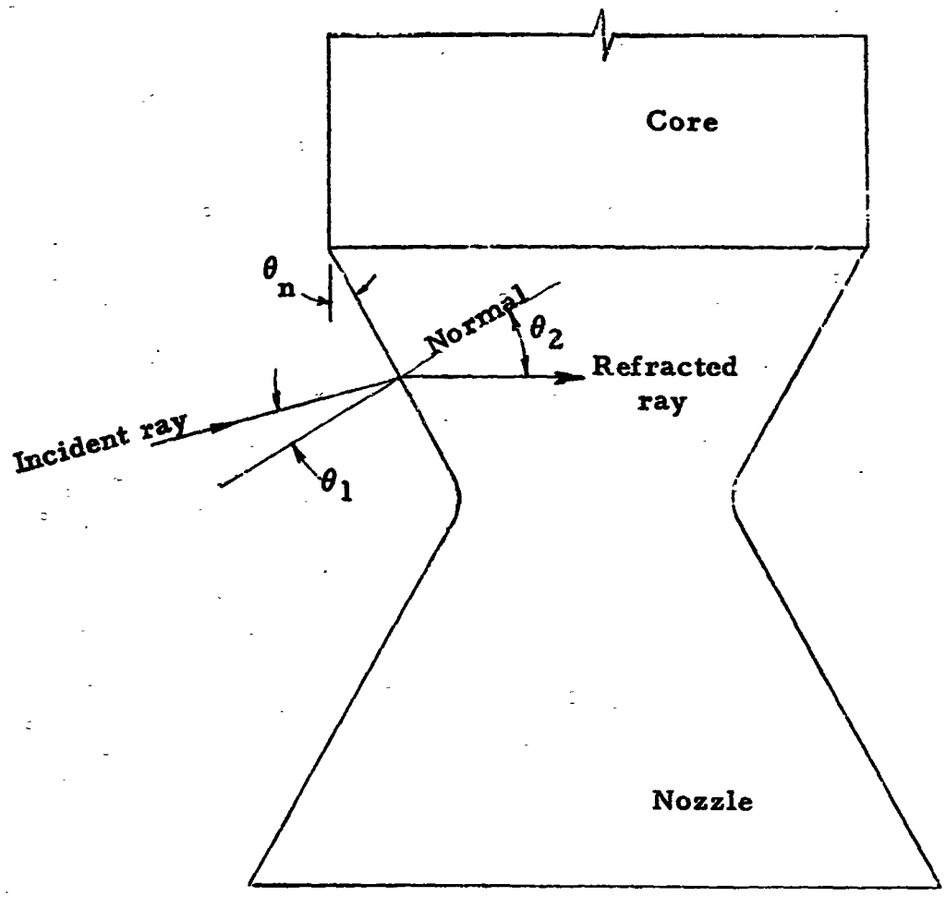

Figure 33. Geometry and notation for analysis of refraction effects in exhaust gas.

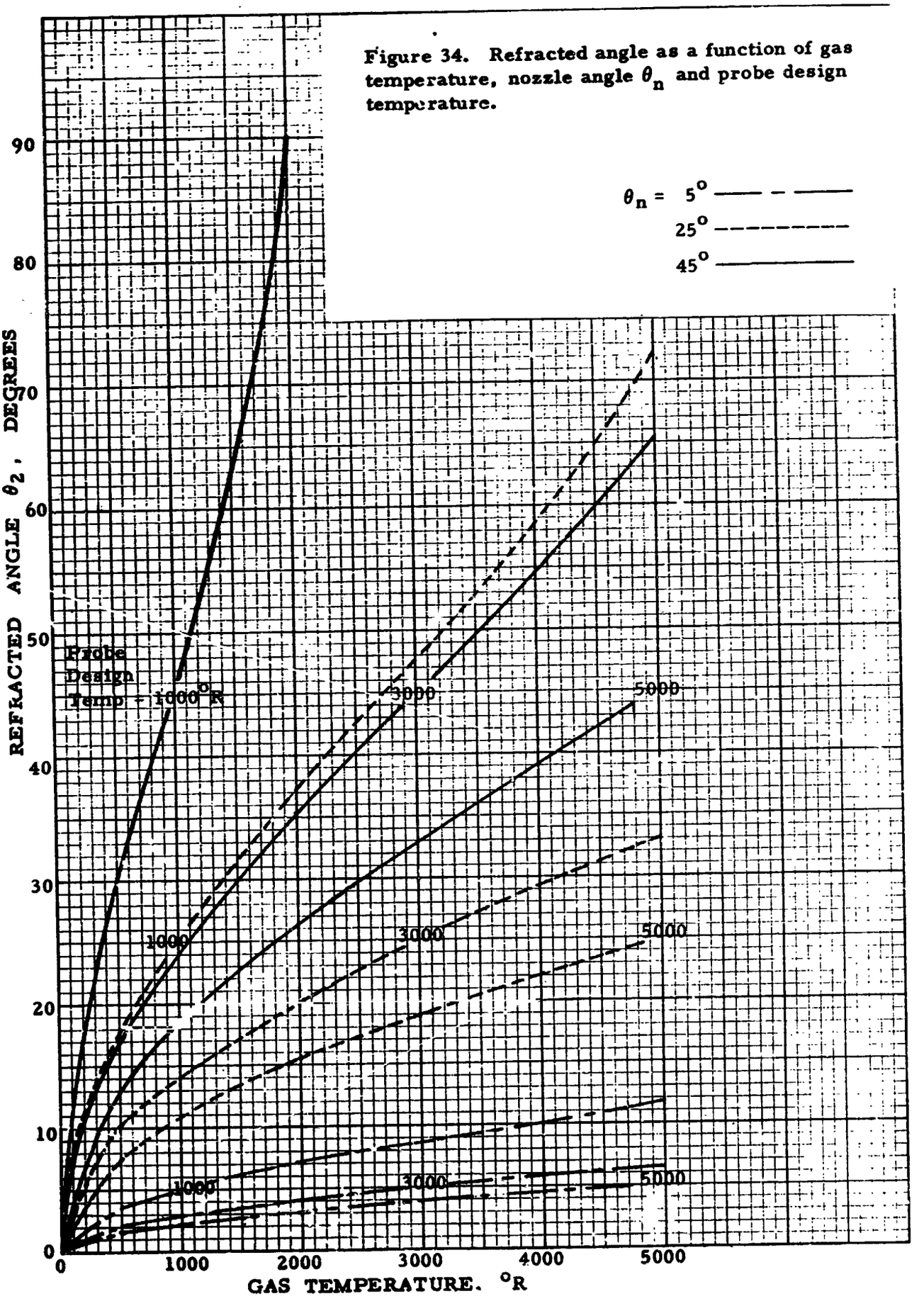

Figure 34. Refracted angle as a function of gas temperature, nozzle angle θ_n and probe design temperature.

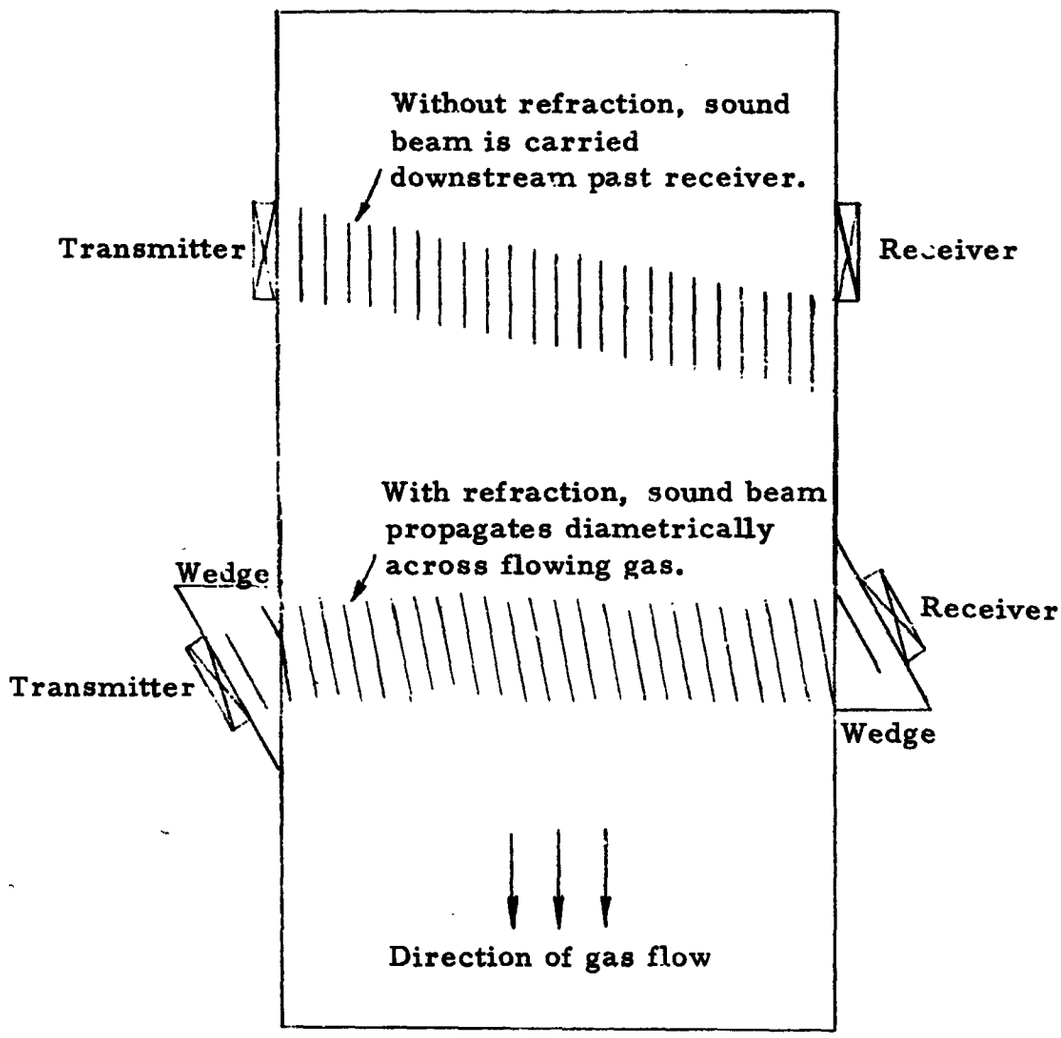

Figure 35. Beam steering using refraction effects to compensate for gas flow.

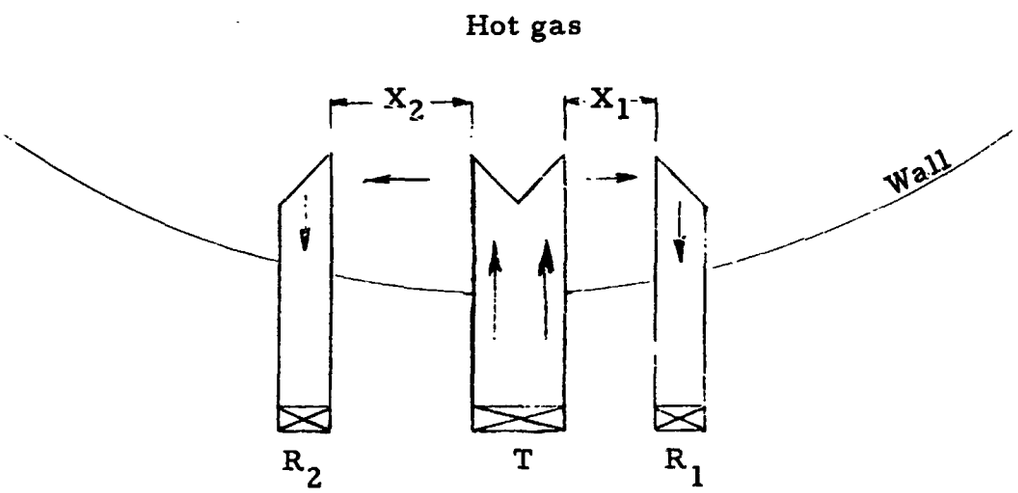

Figure 36. Ultrasonic measurement of local gas temperature near wall.

(a) Transit time measured over parallel chords.

(b) Transit time measured over nonparallel chords.

Figure 37. Ultrasonic measurement of radial temperature distribution.

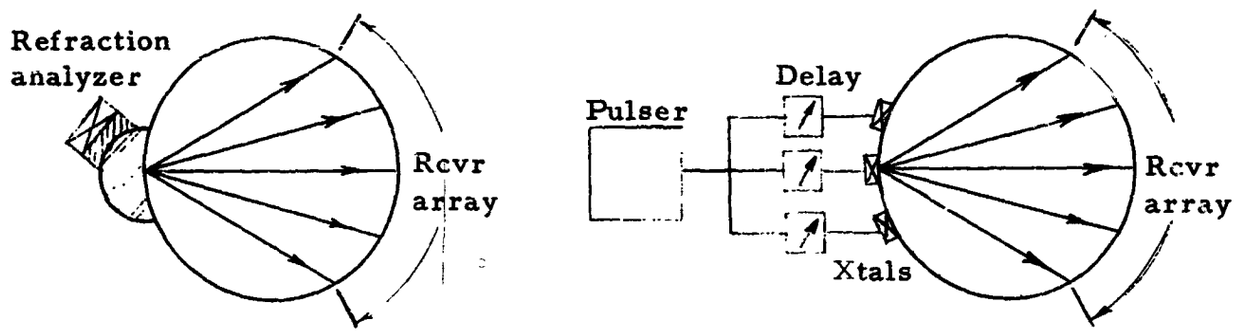

(a) Mechanical steering

(b) Electrical steering

Figure 38. Ultrasonic beam steered to different receivers.

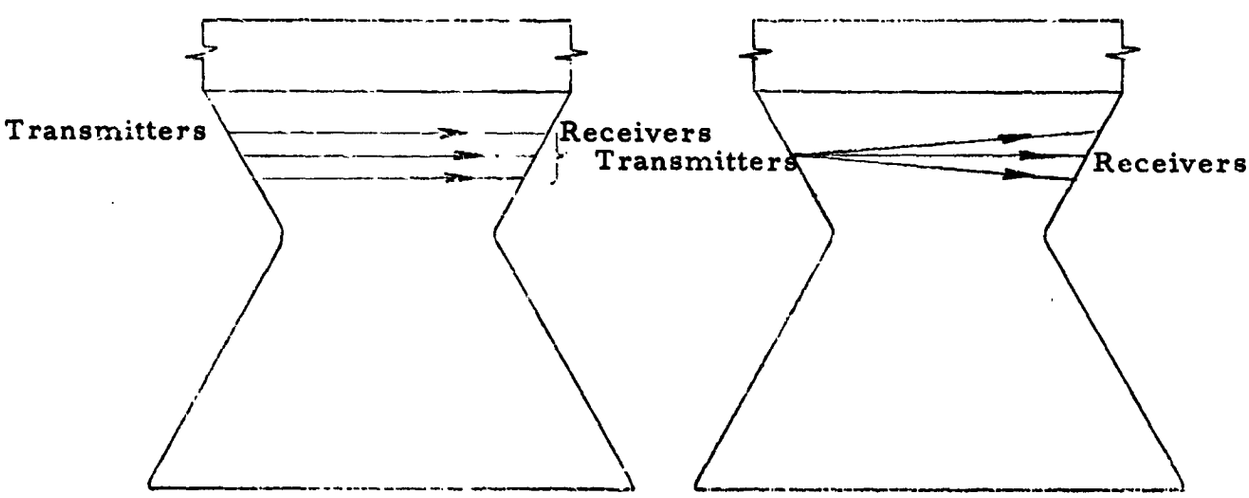

(a) Parallel acoustic paths

(b) Nonparallel acoustic paths

Figure 39. Ultrasonic measurement of axial temperature distribution.

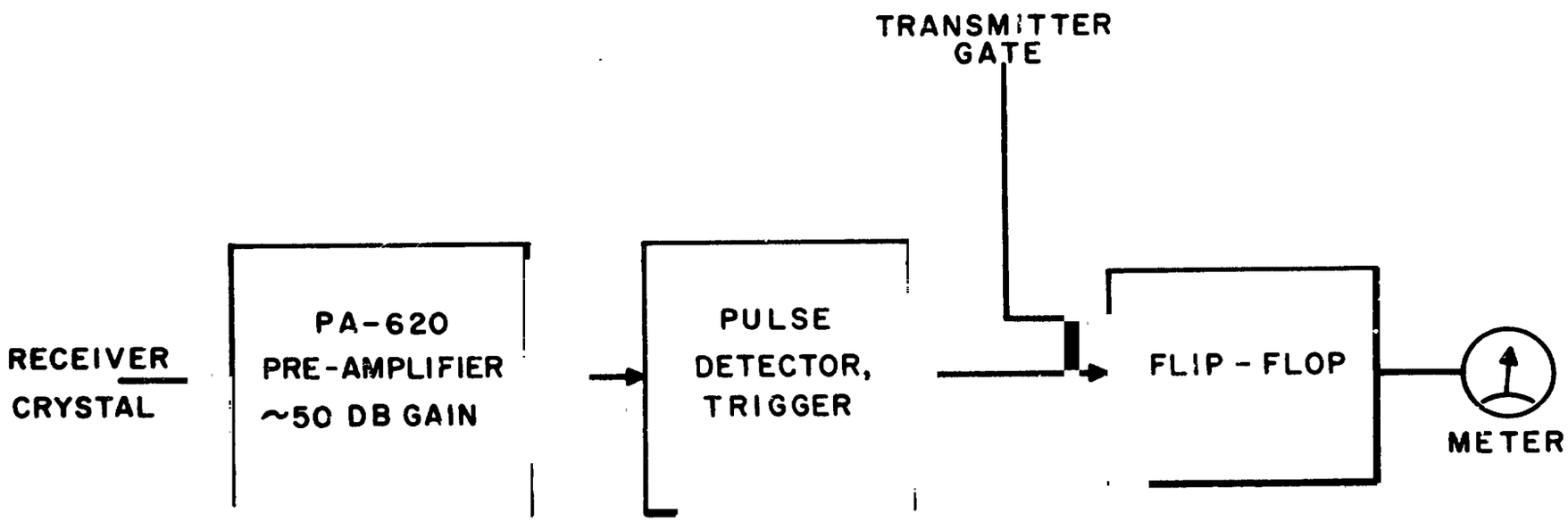

FIG. 40: ANALOG OUTPUT GENERATOR

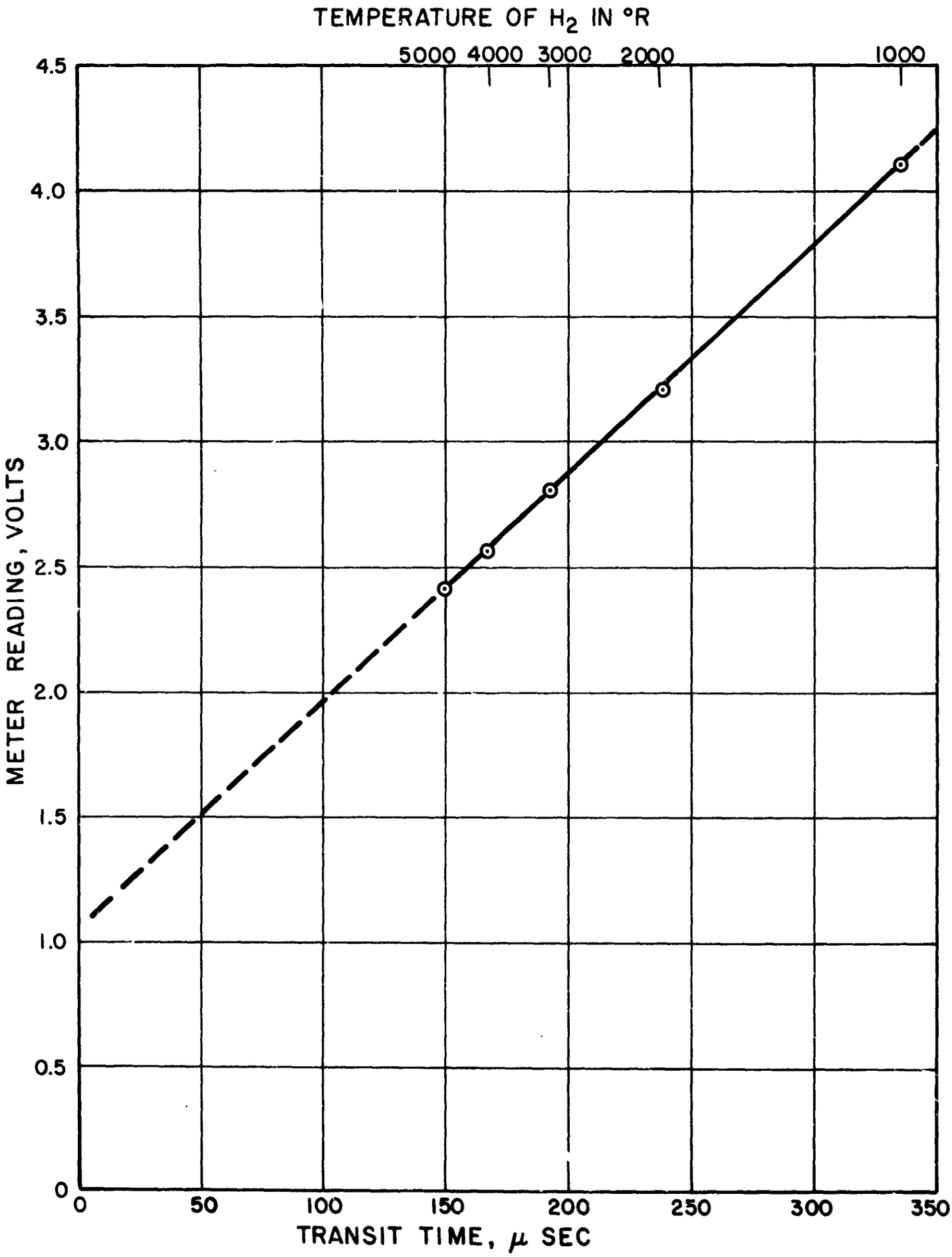

Figure 1. Ultrasonic thermometer calibration.